Journal of Structural Geology 32 (2010) 2042–2071

Contents lists available at ScienceDirect

Journal of Structural Geology

journal homepage: www.elsevier.com/locate/jsg

Review Article

Information from folds: A review

Peter J. Hudleston [a,*], Susan H. Treagus [b]

[a] Department of Geology and Geophysics, University of Minnesota, Minneapolis, MN 55455, USA
[b] School of Earth, Atmospheric and Environmental Sciences, University of Manchester, Manchester M13 9PL, UK, England

ARTICLE INFO

Article history:
Received 13 January 2010
Received in revised form
24 July 2010
Accepted 22 August 2010
Available online 8 September 2010

Keywords:
Folds
Folding
Deformation history

ABSTRACT

Folds are spectacular geological structures that are seen in layered rock on many different scales. To mark 30 years of the Journal of Structural Geology, we review the information that can be gained from studies of folds in theory, experiment and nature. We first review theoretical considerations and modeling, from classical approaches to current developments. The subject is dominated by single-layer fold theory, with the assumption of perfect layer-parallel shortening, but we also review multilayer fold theory and modeling, and folding of layers that are oblique to principal stresses and strains. This work demonstrates that viscosity ratio, degree of non-linearity of the flow law, anisotropy, and the thickness and spacing distribution of layers of different competence are all important in determining the nature and strength of the folding instability. Theory and modeling provide the basis for obtaining rheological information from natural folds, through analysis of wavelength/thickness ratios of single layer folds, and fold shapes. They also provide a basis for estimating the bulk strain from folded layers. Information about folding mechanisms can be obtained by analysis of cleavage and fabric patterns in folded rocks, and the history of deformation can be revealed by understanding how asymmetry can develop in folds, by how folds develop in shear zones, and how folds develop in more complex three-dimensional deformations.

1. Introduction

Folds are spectacular structures in deformed rocks, affecting single or multiple layers on all scales, and on a small-scale commonly seen affecting veins, schistosities and foliations (Figs. 1 and 2). They have played an important part, historically, in understanding episodes of deformation in orogenic belts. To mark 30 years of the Journal of Structural Geology, we combine forces and indulge our separate love of folds to review the information that can be gained from studies of folds in theory, experiment and nature.

It was probably Hall (1815) who first used the word *folds* in connection with rock structures. He was describing the models he had made from layered cloths confined between boards and laterally compressed, to simulate folded rocks he had observed on the Berwickshire coast of Britain. He wrote: "The consequence was … the strata were constrained to assume folds, bent up and down, which very much resemble the convoluted beds … exhibited in the crags of Fast Castle". Among the early studies of folds are the outstanding contributions of Willis (1891) on mechanics and terminology and Van Hise (1894) on geometry. Much of the work on folds in the first half of the 20th century was concerned with developing geometrical methods for representing folds. Details can be found in the textbooks of Leith (1923), Nevin (1931), Hills (1963) and de Sitter (1964). A review of work on the mechanics of folding through the mid 1970s can be found in Johnson (1977: Chapter 1).

In this review, we concentrate on the *information* that folded rocks and their analysis can provide: information on rheology, strain and deformation history, locally or regionally. Much of this information stems from developments in fold theory and modeling over the course of the last 50 years, beginning with the work of Biot (1961, 1965a, 1965b), who developed theories for single and multilayer folding in viscoelastic and viscous media, with applications to rocks, Currie et al. (1962), who developed models of elastic folding and structural lithic units that were related to folds in the Appalachians, and Ramberg (1959, 1963, 1964, 1970), who made significant contributions to the modern understanding of folding mechanisms, based on theory and model experiments. These studies together form the foundations of modern fold theory and modeling, expanded below.

In their papers on buckling, Biot (1961, 1965a) and Ramberg (1964, 1970, 1981) extended their analysis to include the influence of gravity. In this paper we do not consider gravitational forces, which may become important for large folds, and are certainly so for folds that affect the earth's surface. In the last

* Corresponding author.
E-mail addresses: hudle001@umn.edu (P.J. Hudleston), susan.h.treagus@manchester.ac.uk (S.H. Treagus).

0191-8141/$ – see front matter © 2010 Elsevier Ltd. All rights reserved.
doi:10.1016/j.jsg.2010.08.011

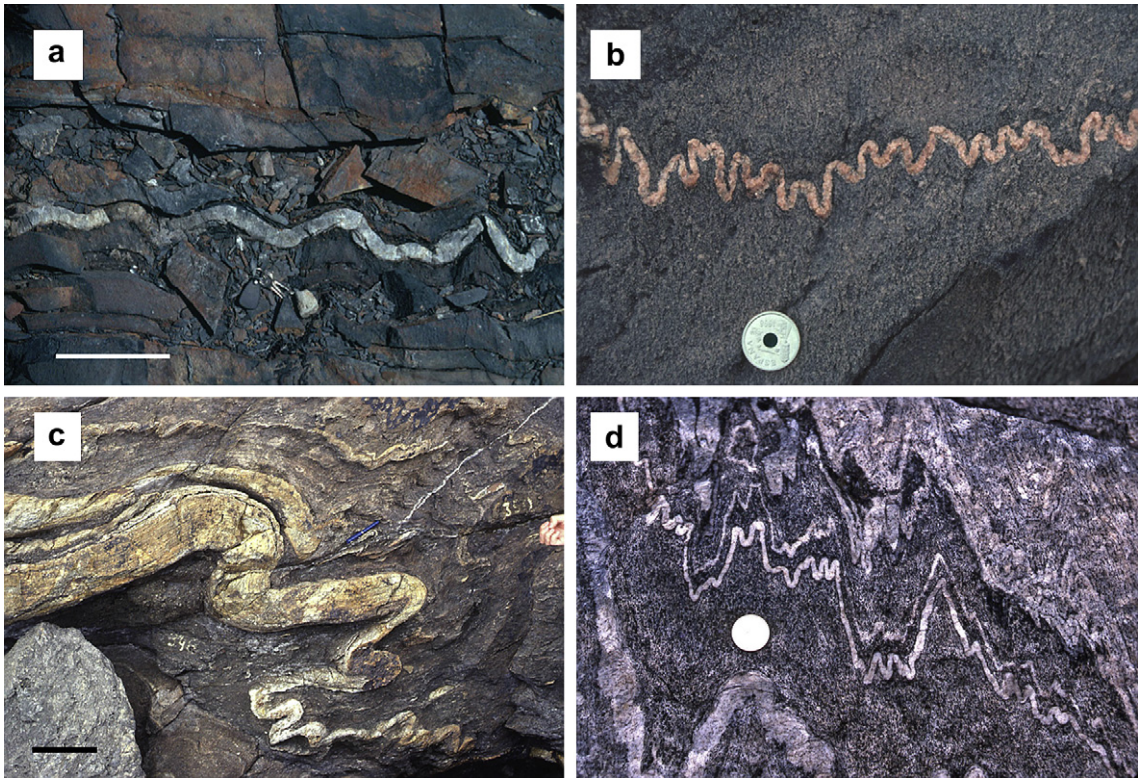

Fig. 1. Examples of small-scale buckle folds. (a) Quartz veins in slate, Trondheim, Norway; scale bar 20 cm. (b) Quartz veins in schist, Cap de Creus, Spain; coin 2 cm. (c) Mylonitized pegmatite vein in mylonites, Cap de Creus, Spain, showing wavelength decreasing with thickness; scale bar 10 cm. (d). Single-layer buckling in thin white pegmatitic veins modified by multilayer effects of banding in gneisses of the Maggia nappe, Ticino, Switzerland; coin 2.3 cm.

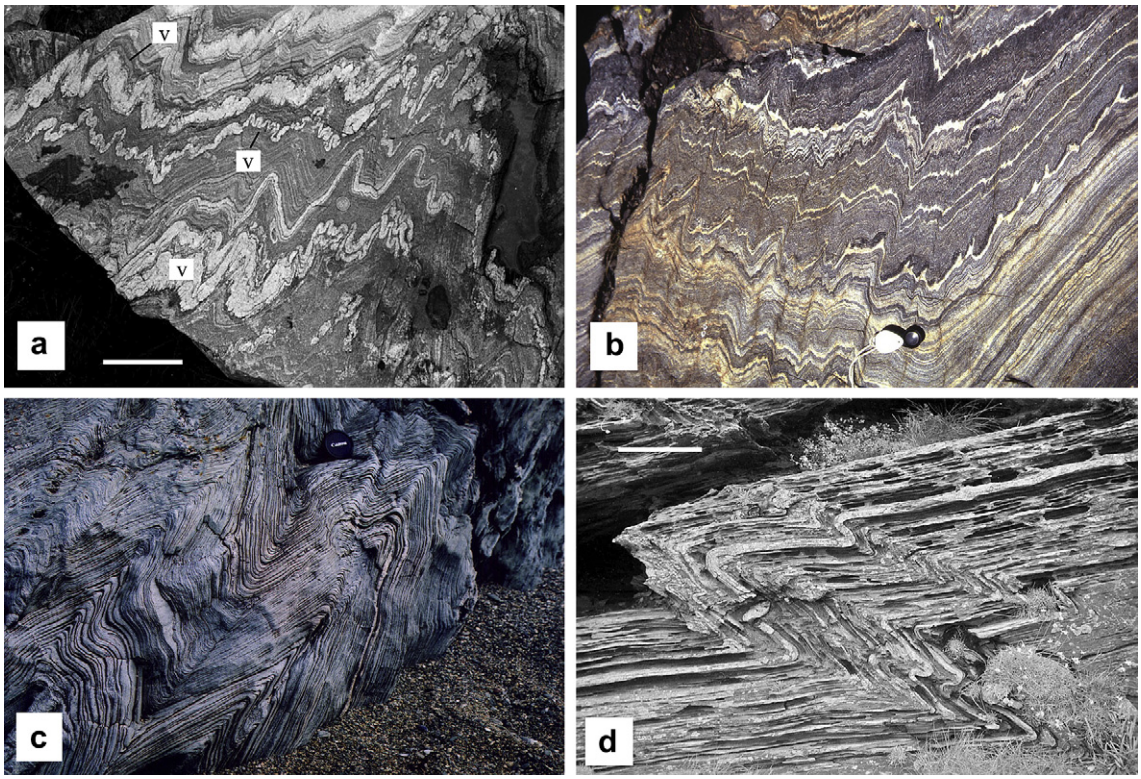

Fig. 2. (a) Multilayer folds in Moine schists, with wavelengths determined by competent white quartzo-feldspathic veins of different thickness (v) that have buckled largely independently; Loch Monar, Scotland; scale bar 20 cm. (b) Multilayer folds in anisotropic gneiss, Maggia nappe, Ticino, Switzerland; hand lens 5 cm. (c) Multilayer folding in the New Harbour Formation psammitic schists, Silver Bay, Anglesey, UK; lens cap 5 cm. (d) Multilayer buckle folds of chevron style and variable asymmetry in siltstone and slates, Boscastle, Cornwall, England; scale bar 20 cm. The overall fold style is similar (Class 1C, Ramsay, 1967, p. 367), but the stiff siltstone layers have parallel shapes (Class 1B).

decade or so, work on large-scale buckle folding has focused on the whole lithosphere (e.g. Burg and Podladchikov, 1999; Cloetingh et al., 2002), at which scale gravitational forces are of great importance.

2. Theoretical considerations and modeling

2.1. Single-layer fold theory

Single layer fold theory concerns the buckling of isolated layers subjected to layer-parallel compression, developed for the case of a stiff or competent viscous layer in a less stiff or less competent matrix (Biot, 1961; Biot et al., 1961; Ramberg, 1961, 1963; Chapple, 1968; Fletcher, 1974, 1977; Smith, 1975, 1977, 1979; Johnson and Fletcher, 1994) and for the corresponding cases of elastic and viscoelastic layers and matrix (Biot, 1961, 1965a; Currie et al., 1962; Johnson, 1977; Mühlhaus et al., 1994, 1998; Hunt et al., 1996, 1997; Schmalholz and Podladchikov, 1999, 2000; Jeng and Huang, 2008). Classical theory predicts that if the layer is given small sinusoidal perturbations of different wavelengths, one such perturbation will amplify at a greater rate than all others. The wavelength of this perturbation is termed the *dominant wavelength*, λ_d. For Newtonian viscous layer and matrix in plane strain, with maximum shortening parallel to the layer and ignoring gravity and inertial effects, λ_d depends only on the ratio of viscosities of layer to matrix. The thin-plate (see below) approximation for λ_d is:

$$\frac{\lambda_d}{h} = 2\pi\left(\frac{\mu_L}{6\mu_M}\right)^{1/3}, \tag{1}$$

where h is layer thickness and μ_L and μ_M the viscosities of layer and matrix (Biot, 1961; Ramberg, 1961). This approximation holds for both welded and free-slip contacts between layer and matrix. It is good for $\mu_L/\mu_M \geq 100$, but becomes increasingly inaccurate as μ_L/μ_M is decreased and the assumptions of the thin plate formulation become untenable. (Note in this regard that Eq. (1) gives a dominant wavelength for the case when $\mu_L/\mu_M = 1$, which is not physically meaningful).

Under suitable conditions, including sufficiently large strain rates, the elastic properties of rocks may influence the folding instability. The thin-plate expression for the dominant wavelength of an elastic layer in an elastic matrix is identical in form to Eq. (1) (e.g., Currie et al., 1962; Jeng and Huang, 2008).

$$\frac{\lambda_d}{h} = 2\pi\left(\frac{E_L}{6E_M}\right)^{1/3}, \tag{2}$$

where E_L and E_M are the elastic moduli of layer and matrix. Elastic behavior by itself is obviously inappropriate for rocks, in which folds represent permanent inelastic deformation. If an elastic layer is embedded in a viscous matrix, the dominant wavelength is dependent on applied load (or alternatively rate of deformation). It is given by:

$$\frac{\lambda_d}{h} = \pi\left(\frac{E_L}{P(1-\nu_L^2)}\right)^{1/2}, \tag{3}$$

where ν_L is Poisson's ratio and P is the layer-parallel stress in the stiff layer (Biot, 1961; Turcotte and Schubert, 1982). Note that the dominant wavelength in this case is independent of the viscosity of the matrix. If the layer is viscoelastic (Maxwell rheology, equivalent to a spring and a dashpot in series) and the matrix viscous, Schmalholz and Podladchikov (1999) showed that whether the folding is controlled largely by its viscous properties (with λ_d given by Eq. (1)) or largely by its elastic properties (with λ_d given by Eq. (3)) depends on the ratio of the viscous to elastic dominant wavelengths. If the ratio, $R = \lambda_{dv}/\lambda_{de} < 1$, λ_d is given approximately by Eq. (1) and if $R = \lambda_{dv}/\lambda_{de} > 1$, λ_d is given approximately by Eq. (3).

A *buckling instability* is in fact one of a family of dynamic instabilities that result from either compression or extension of an isolated layer that is either more or less viscous than its matrix, as shown by Smith (1975, 1977). Folding is by far the strongest of these four instabilities and the only one considered here. The other important instability is that of pinch and swell or boudinage that results from extension of a stiff layer in a less competent matrix, and this instability is only significant if the material behavior is non-linear, because for Newtonian materials the dynamic growth is counteracted by the kinematic decay associated with the base flow. However, if the base flow involves extension along the axes of the boudins, it may be possible to produce boudinage in Newtonian flow (James and Watkinson, 1994).

Thin-plate analysis takes into account only normal stresses in the competent layer, and the stresses associated with folding consist of deviatoric tension in the outer arcs and deviatoric compression in the inner arcs (Fig. 3). Layer-parallel shear stress is ignored. *Thick plate analysis* does not make this restrictive assumption about stresses (Johnson and Fletcher, 1994, pp. 196–207), and thus provides more accurate predictions of the dominant wavelength at low viscosity contrast and for low-amplitude fold growth. *Third order analysis* of the problem (Johnson and Fletcher, 1994, pp. 224–236) accounts for the deviation of the layer shape of the growing fold from sinusoidal. Thick plate analysis does not lead to an explicit expression for the dominant wavelength. In viscous materials, whether thin-plate or thick-plate analysis is used, the layer will shorten and thicken under the influence of the compressive normal stress (Fig. 4), and treating this analytically involves considering the stresses in the layer to consist of two parts, a uniform stress that results in shortening of the layer with time and a perturbation stress field that is the source of the buckling instability (see Fig. 3 for the thin-plate case). At high viscosity contrasts the amount of shortening that will occur before the folds grow to finite amplitude is small, but at low viscosity contrasts significant layer-parallel shortening will occur as the folds amplify.

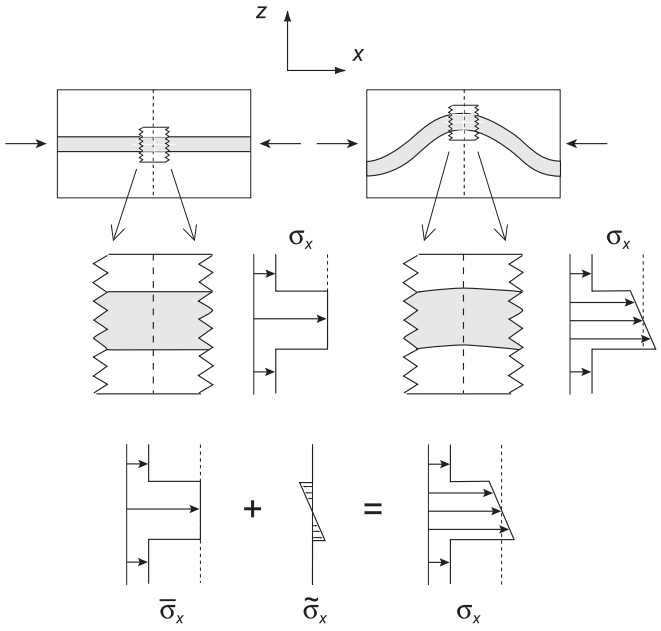

Fig. 3. In thin-plate analysis, the normal stress, σ_x, in the layer can be considered the sum of a uniform (membrane) stress, $\bar{\sigma}_x$, and fiber stresses, $\tilde{\sigma}_x$, related to the perturbation of the layer (after Schmalholz and Podladchikov, 2000).

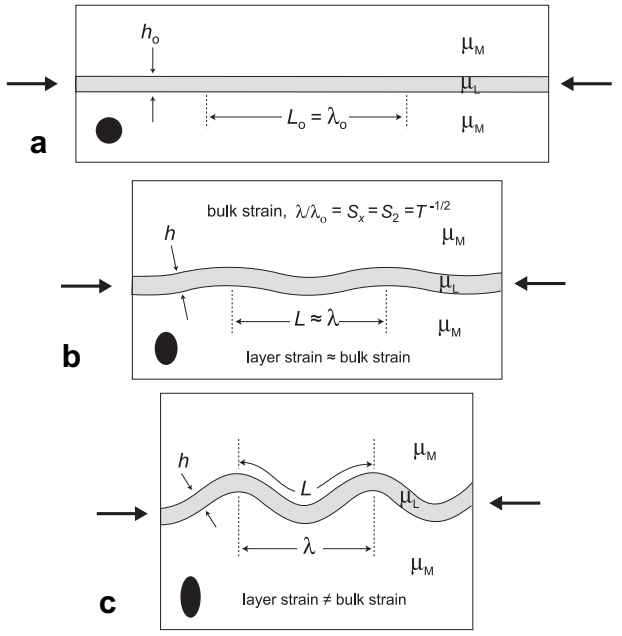

Fig. 4. Definition of terms used to described periodic folds at various stages of development. (a) Initial state; (b) after fold nucleation and growth and towards the end of wavelength selection; (c) after growth to large amplitude. If $L \approx \lambda_p$ at stage (b), L in (c) is a rough measure of λ_p at the strain shown in (b) (see text).

Ramberg (1964) emphasized the implications of this for single layers with different values of μ_L/μ_M deformed under the same conditions of overall shortening – the layers will appear to have undergone different degrees of folding. At very low viscosity contrasts the *kinematic* amplification, due only to the geometric change associated with homogeneous strain, masks the *dynamic* amplification due to the buckling instability.

Sherwin and Chapple (1968) modified thin plate theory to take into account the effect of layer-parallel shortening that accompanies low-amplitude fold growth. In this case, the wavelength of the folds with the greatest cumulative amplification is a function of the layer-parallel shortening. Johnson and Fletcher call this the *preferred wavelength*, λ_p. The approximate (thin-plate) expression for λ_p is:

$$\frac{\lambda_p}{h(T)} = 2\pi\left(\frac{\mu_L}{6\mu_M}\frac{T+1}{2T^2}\right)^{1/3}, \tag{4}$$

where $T = S_1/S_2 = S_1^2$, and S_1 and S_2 are the principal stretches perpendicular and parallel to the layer respectively. From Biot (1965a, p. 427), and Johnson and Pfaff (1989) it can be shown that:

$$\frac{\lambda_p}{h} = \frac{\lambda_d}{h_o}S_2. \tag{5}$$

The analyses discussed above assume a form of linear viscous or viscoelastic rheology. However, experiments on common rock-forming minerals and rocks, and fabric analyses in naturally-deformed rock, suggest that under certain conditions of ductile deformation, rocks might be expected to follow non-linear flow laws (e.g. Carter and Tsenn, 1987; Kirby and Kronenberg, 1987; Rutter, 1993; Kohlstedt et al., 1995; Hirth et al., 2001). Fletcher (1974) and Smith (1975, 1977) independently developed the theory for *folding of layers with non-linear rheology*, in the case of Fletcher specifically power-law, for which the single component stress – strain rate relationship is of the form $\dot{e} = B\sigma^n$, where n is the power-law exponent and B a constant. An approximate expression for the dominant wavelength corresponding to the thin-plate expression, Eq. (1), is (Fletcher, 1974):

$$\frac{\lambda_d}{h} = 2\pi\left(\frac{\mu'_L}{6\mu'_M}\frac{n_M^{1/2}}{n_L}\right)^{1/3}, \tag{6}$$

where n_L and n_M are the power-law exponents and μ'_L and μ'_M the viscosities under the base rate of flow (in response to the stress $\overline{\sigma}_x$ in Fig. 3) for the layer and matrix respectively. Note that for power-law fluids it is not meaningful to talk about a single viscosity contrast between two rock types because viscosity varies as function of stress or strain rate, and thus viscosity ratio will vary as stress or strain-rate vary (Treagus, 1993).

Another important rock property that affects the folding instability is *anisotropy*. As pointed out by Fletcher (1974), power-law rheology and anisotropy of the competent layer, in which the viscosity of the layer in shear parallel to the layer is less than the viscosity in shortening or extension, have opposite effects on the secondary flow associated with folding and thus on the buckling instability. The stress-induced anisotropy of the secondary flow associated with power-law rheology involves the layer becoming weaker in compression than in shear, whereas the intrinsic anisotropy of layered rocks involves the layer being weaker in shear parallel to the layer than in compression. Anisotropy of this type in the competent layer lessens the buckling instability, whereas anisotropy in the matrix increases it, compared to the isotropic case and if normal viscosities of layer and matrix are kept fixed (Kocher et al., 2006).

In general, for viscous materials the rate of growth of a sinusoidal perturbation can be expressed by a function of the following form (Fletcher, 1974):

$$\frac{dA}{d\tau} = [1 + q(k)]A(k), \tag{7}$$

where A is amplitude, $q(k)$ is a growth factor, $k = 2\pi h/\lambda$, and τ is dimensionless time ($\tau = -\dot{e}_x t$, where $\dot{e}_x$ is the base strain rate corresponding to the stress $\overline{\sigma}_x$, t is time and $e^{2\tau} = T$). This implies an exponential increase in fold amplitude with time or with shortening strain. Using $e^{2\tau} = T$ and changing and separating variables the expression for amplification becomes:

$$\ln\frac{A}{A_o} = \int_1^T [1 + q(k)]\,\frac{1}{2T}dT, \tag{8}$$

where A_o is initial amplitude. The value of $q(k)$ depends on the rheological properties and implies mechanical instability if greater than zero. A value of $q = 0$ describes purely kinematic amplification. For a given set of rheological parameters, $q(k)$ attains a maximum value for the dominant wavelength. Exact first order expressions for $q(k)$ have been derived for linear rheology under conditions of bonded-contact and free-slip layer interfaces by Johnson and Fletcher (1994, pp. 196–206) and for bonded-contact power-law rheology (Fletcher, 1974; Johnson and Fletcher, 1994, p. 383). Results for linear rheology, bonded contacts and three values of μ_L/μ_M are shown in Fig. 5a, and values of the dominant wavelength/thickness, λ_d/h, as a function of viscosity contrast are shown in Fig. 5b, where the differences between thin-plate and exact solutions with either bonded or free-slip contacts can be compared. Thin-plate theory overestimates the growth rate and underestimates the value of λ_d/h for a given viscosity contrast.

The variations of $q(k)$ with λ/h for a viscosity ratio of 50 and for both linear and power-law behavior of the layer and isotropic and anisotropic behavior of the matrix are shown in Fig. 6. The

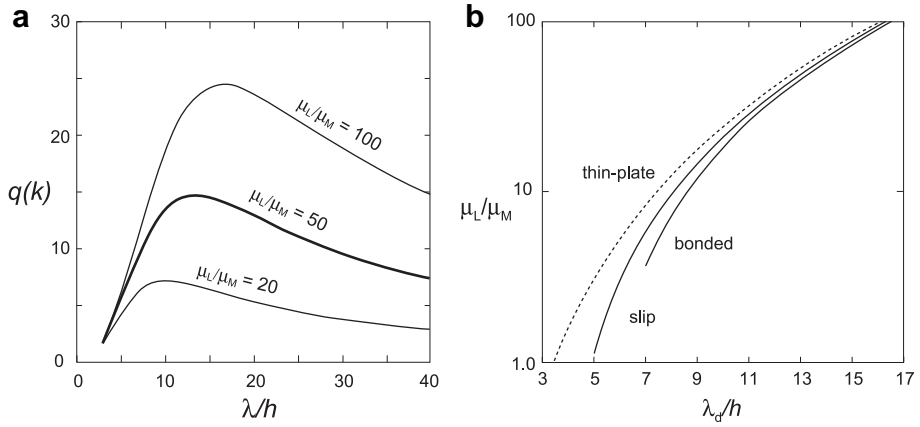

Fig. 5. (a) Growth factor, $q(k)$ (Johnson and Fletcher, 1994, Eq. 5.2.12b) as a function of λ/h for linear viscous layer and matrix (bonded contacts) and three different viscosity contrasts. (b) Dominant wavelength/thickness, λ_d/h, as a function of viscosity ratio for an isolated single layer, for the thin-plate (Biot) approximation and for exact thick-plate first order solutions with either bonded or free-slip contacts and linear viscosity (Eq. (1), and from Johnson and Fletcher, 1994, Eqs. 5.2.16b, 5.2.17).

growth rate curves in this figure were obtained from Fletcher (1974, Eq. 8):

$$q(k) = 2n_L(1-R')\Big\{-\left(1-Q^2\right)+\sqrt{n_L-1}\Big[(1+Q)^2e^{\alpha_L k} - (1-Q)^2e^{-\alpha_L k}\Big]\Big/2\sin(\beta_L k)\Big\}^{-1}, \quad (9)$$

where $R' = \mu'^{n}_{M}/\mu'^{n}_{L}$, $R'' = \sqrt{\mu'^{n}_{M}\mu'^{s}_{M}}/\mu'^{n}_{L}$, $Q = \sqrt{n_L}R''$, $\alpha_L = \sqrt{1/n_L}$, and $\beta_L = \sqrt{1-1/n_L}$. Fletcher (1974) pointed out, following Biot (1965a, p. 211), that for single-layer folding, an anisotropic viscous matrix behaves like an isotropic viscous half-space with effective viscosity $\mu = \sqrt{\mu^n\mu^s}$. This allows Eq. (9) to be used to incorporate the effect of an anisotropic matrix. It is clear from Fig. 6 that power-law behavior of the layer both enhances the growth rate and decreases the dominant wavelength compared to linear behavior, whereas anisotropy of the matrix increases both the growth rate and the dominant wavelength. A combination of power-law layer and anisotropic matrix greatly enhances growth rates and modestly affects the dominant wavelength. The degree to which the growth rate and dominant wavelength are affected

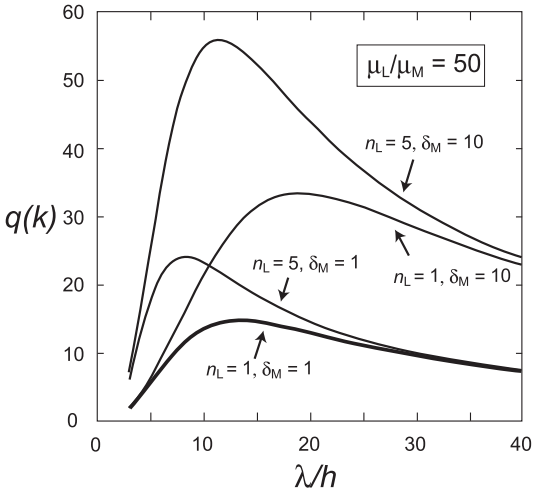

Fig. 6. Effect of power-law rheology of layer and anisotropy of matrix on dynamic growth rates and dominant wavelength (given by λ/h for the peak values of these curves) of single layer buckle folds. n_L is the power-law exponent of the layer and $\delta_M = \mu'^{n}_{M}/\mu'^{s}_{M}$ (with μ'^{n}_{M} and/μ'^{s}_{M} being the normal and shear viscosities of the matrix) is the anisotropy factor of the matrix (see Kocher et al., 2006). In all cases the ratio of normal viscosity of the layer to the normal viscosity of the matrix, $\mu'^{n}_{L}/\mu'^{n}_{M} = 50$.

obviously depends on the power-law exponent and the degree of anisotropy. An analytical solution for an anisotropic layer in an isotropic matrix has been derived by Fletcher (personal communication), and this and numerical simulations (Kocher et al., 2006, Fig. 2c), show that the growth rate for an anisotropic layer is suppressed compared to the linear case, for fixed μ^n_M/μ^n_L.

Using the appropriate expression for $q(k)$, Eq. (8) can be integrated numerically over the path $k(\tau) = k_o e^{2\tau} = k_o T$ to find the cumulative amplification, A/A_o, of folds with initial wave number, k_o. By creating spectra of A/A_o as a function of k the value $k_p = 2\pi h/\lambda_p$that shows the maximum cumulative amplification can be found. An example of amplification spectra for increasing amounts of shortening is shown in Fig. 7 for Newtonian layer and matrix. An exact expression for k_p or λ_p/h was derived by Sherwin and Chapple (1968) for the thin-plate linear viscous case (Eq. (4)).

2.2. Finite amplitude single-layer fold theory

First-order buckling theory predicts an exponential increase in amplitude with time or shortening (Eqs. (7) or (8)) as folding initiates and is strictly applicable only for infinitesimal amplitudes. Extending theoretical analysis beyond first order (Fletcher, 1979; Johnson and Pfaff, 1989; Johnson and Fletcher, 1994, pp. 224–236), shows that higher waveforms spontaneously develop that serve to modify fold shape and limit the growth rate of the first waveform. Cruikshank and Johnson (1993) developed a method of matching boundary conditions along irregular interfaces that allows fold development to be predicted accurately to high amplitudes. Schmalholz and Podladchikov (2000) developed a simple modification of the thin-plate theory for single layers that effectively tracks fold amplitude, without specifying the exact fold shape. This takes into account the fact that for fold growth to continue exponentially, according to the linear theory, a stretching of the competent layer would have to occur, and it is resistance to this stretching that slows fold growth. They assumed that the layer-parallel stress (membrane stress, $\overline{\sigma}$ in Fig. 3) in the competent layer remains constant around the layer as the fold grows to finite amplitude but decreases with time in response to the resistance of the layer to stretching. The membrane stress is related to layer-parallel (arclength) strain rate, which is therefore also constant around the layer. Both membrane stress and strain rate will decrease as the fold grows, and analytical expressions for these were obtained by Schmalholz and Podladchikov (2000), expressing membrane stress as a function of initial stress and arc strain rate as

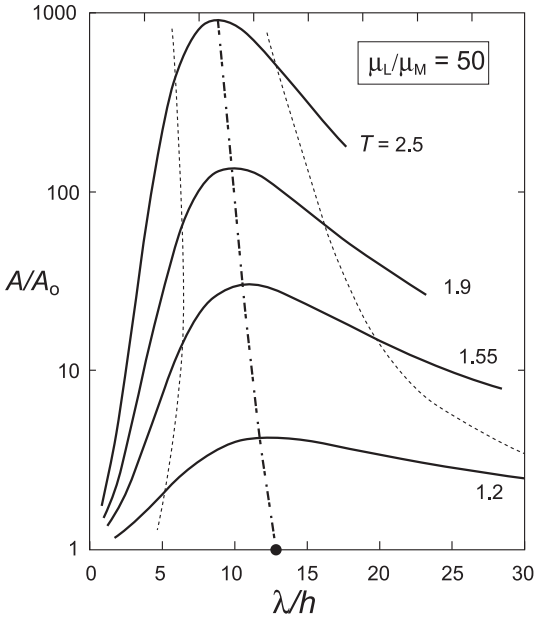

Fig. 7. Amplification spectra for $\mu_L/\mu_M = 50$ (Newtonian, isotropic) after increasing amounts of shortening strain, $T = S_1/S_2$, during low-amplitude fold growth. The black dot shows the dominant wavelength/thickness, λ_d/h, and the dash-dotted line tracks the change in preferred wavelength/thickness, λ_p/h, with shortening. The dashed lines track wavelengths that have been amplified to half the maximum value. They show the increased selectivity of amplification with shortening.

a function of initial or background strain rate. A comparison of first order (small amplitude) theoretical predictions of fold growth with the predictions of Schmalholz and Podladchikov's (2000) finite amplitude theory is made in Fig. 8. The finite amplitude theory agrees very well with numerical simulations of buckling (see Schmalholz and Podladchikov, 2000, Fig. 6), which do not depend on thin-plate assumptions about stress in the competent layer. The amount of strain accumulated in the stage during which the exponential curves track fold growth depends on the amplitude of the initial perturbation in the layer – the smaller the initial perturbation, the greater the amount of strain. In general it is quite limited.

The departure of the finite-amplitude growth curve from the infinitesimal-amplitude growth curve is reflected in a transition from layer shortening accompanying exponential growth to fold growth with little change in layer (arc) length. This is shown in Fig. 9. Schmalholz and Podladchikov (2000) proposed the term *crossover amplitude* for the amplitude at which this transition occurs. They also proposed the term *nucleation amplitude*, which is the amplitude at which the dynamic rate of fold growth is equal to the kinematic rate. Both nucleation amplitude and crossover amplitude have precise definitions, and depend only on the growth rate factor, $q(k)$, (Schmalholz and Podladchikov, 2000, Eq. (16); Schmalholz and Podladchikov, 2001, Eq. (8)).

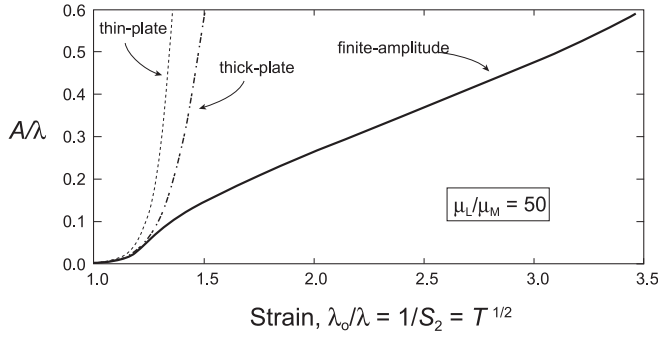

Fig. 8. Growth of fold amplitude/wavelength, A/λ, for a single layer with $\mu_L/\mu_M = 50$ and with initial sinusoidal perturbation of the dominant wavelength ($\lambda_d/h = 12.75$) and initial amplitude equal to 0.02 of layer thickness, according to thin-plate theory (Biot, 1961), thick-plate theory (Fletcher, 1974) and finite amplitude theory of Schmalholz and Podladchikov (2000). The predictions of the finite amplitude theory are closely matched by 2D numerical simulations (Schmalholz and Podladchikov, 2000).

2.3. Single-layer fold modeling: analog and numerical

Considerable experimental work has been done to investigate the nature of folding instabilities in single stiff layers embedded in a less stiff matrix and subjected to layer-parallel shortening, using a variety of analog materials for layer and matrix. The existence of a characteristic or quasi-characteristic wavelength in physical model experiments, and good correspondence with theoretical predictions, have been found experimentally for elastic layers in an elastic matrix (Biot et al., 1961; Currie et al., 1962), elastic layers in viscous matrix (Biot et al., 1961) and viscous layers in viscous matrix, both for Newtonian (Biot et al., 1961; Hudleston, 1973a) and non-Newtonian (Neurath and Smith, 1982; Mancktelow and Abbassi, 1992) cases.

Since digital computers became widely available in the 1960s, numerical methods have been applied with considerable success to study the development of folds to high amplitude. Chapple (1968) used a finite difference approach for this purpose, predicting fold shape in a thin linearly viscous layer of constant length embedded in a viscous matrix. Dieterich (1969) and Dieterich and Carter (1969) used finite element models (FEM) to analyze fold shape, strain distribution and stress history in folds grown to high amplitudes in viscous materials, free from the assumptions of thin-plate theory. Subsequent numerical studies of single-layer folds have included the effects of non-linear rheology (Parrish, 1973; Lan and Hudleston, 1991), anisotropy (Lan and Hudleston, 1996; Kocher et al., 2006), and viscoelastic behavior (Zhang et al., 1996; Mancktelow, 1999; Schmalholz et al., 2001).

Numerical models provide a good means of examining the effects of varying rheological properties and strain rate in a controlled way in viscous and viscoelastic media and also provide an excellent way of testing the dependence of finite fold shape on the initial layer configuration, and in particular on the form of the initial layer irregularities. It is worth noting that essentially identical results

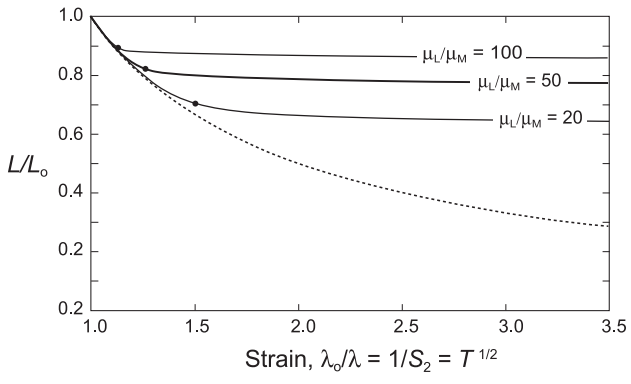

Fig. 9. Change in relative arclength as a function of strain during folding of a single Newtonian layer in Newtonian matrix with an initial sinusoidal (dominant) waveform and initial amplitude of 0.02 of layer thickness, according to the finite amplitude theory of Schmalholz and Podladchikov (2000), for three values of viscosity ratio, μ_L/μ_M. The line for "no folding" represents uniform shortening of the layer without folding. The black dots indicate the *crossover strains*, given by stretch S_c (Schmalholz and Podladchikov, 2000), that approximately limit the stage of folding described by the linear theory.

have been obtained for a wide range of conditions using different numerical techniques. One apparent conflict between results using two different techniques studying buckling in viscoelastic media (see Zhang et al., 1996, who used a finite difference code; and Mancktelow, 1999, who used a finite element code) was due to the fact that different strain rates had been used in the two sets of experiments. When the strain rates were the same, the results of using the two techniques were basically identical (Zhang et al., 2000; Jeng et al., 2002).

Numerical results are consistent with theoretically predicted initial growth rates, which depend on wavelength/thickness of harmonic components, either individually or combined in an imposed initial amplitude spectrum. The results are most clear for *linearly viscous layer and matrix*. If a low-amplitude single waveform is initially present, this will amplify at the theoretically predicted rate, whether or not the waveform is that of the dominant wavelength (Mancktelow, 1999). With initial random perturbations, quasi-periodic folds develop with average wavelength close to the predicted dominant wavelength (Fig. 10, Fletcher and Sherwin, 1978; Mancktelow, 1999; Schmalholz and Podladchikov, 1999, Fig. 3), provided that the amplitudes of the initial irregularities are sufficiently small. The geometry of the final folds does, however, reflect the particular distribution of initial irregularities (e.g. Fig. 10, Mancktelow, 1999, Fig. 17). In non-linear viscous materials, growth rates are enhanced but the final fold form bears a similar relationship to the initial irregularities as for Newtonian materials (e.g. Mancktelow, 1999, Fig. 18).

In nature, folds sometimes occur in packets, and various authors have investigated the growth of folds from an initial isolated perturbation, typically of bell shape (Biot, 1961; Cobbold, 1975, 1977; Abbassi and Mancktelow, 1990) to study how such packets might develop. The phenomenon is referred to as serial folding, and it is observed that folds develop sequentially outwards from the location of the initial perturbation. The wavelength of these folds is close to that predicted by theory for the dominant wavelength (Biot et al., 1961). With enough strain, a packet of high amplitude localized folds may develop (Mancktelow, 1999, Fig. 12). Some authors consider non-linear effects to be important in understanding serial folding (Hunt et al., 1996, 1997, 2006).

If the layers have both *viscous and elastic properties*, the situation is more complicated than when considering viscous properties alone. The behavior of the system then depends not just on viscosity contrast, as for viscous layers, but also on the imposed layer-parallel stress or strain rate. Perhaps the Maxwell model is the most realistic and yet simple constitutive model that has both viscous and elastic properties and that is a good analog for rocks.

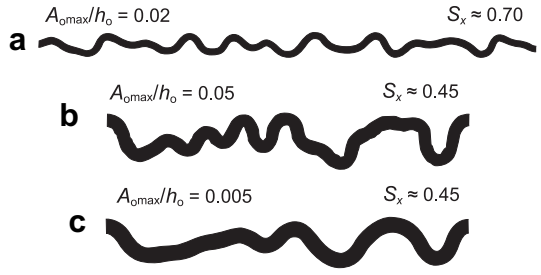

Fig. 10. Examples of single-layer folds produced in numerical models with interfaces possessing random initial irregularities. (a) Linear viscous materials with $\mu_L/\mu_M = 50$ and with initial layer length 15 times the dominant wavelength, and maximum amplitude of irregularities about 0.02 of initial layer thickness, at about 30% shortening (Schmalholz, 2006, Fig. 5a). (b) Viscoelastic layer and matrix, but with fold growth dominated by the viscous properties, with $\mu_L/\mu_M = 50$, and maximum amplitude of initial irregularities 0.05 of initial layer thickness at 55% shortening (Mancktelow, 1999, Fig. 17). (c) The same as (b) but with maximum amplitude of initial irregularities 0.005 of layer thickness (Mancktelow, 1999, Fig. 17).

Schmalholz and Podladchikov (1999) confirmed with numerical models their theoretical prediction that the wavelength of the folds developed in a viscoelastic layer in a viscous matrix depends on the ratio, $R = \lambda_{dv}/\lambda_{de}$, of viscous dominant wavelength (Eq. (1)) to elastic dominant wavelength (Eq. (3)): viscous control when $R < 1$ and elastic control when $R > 1$, as noted earlier (2.1).

In general, *buckling in viscoelastic media* involves consideration of relaxation times of both layer and host, and the situation may be complicated (Mühlhaus et al., 1998; Jeng and Huang, 2008). Jeng et al. (2002, 2008) demonstrated that a waveform of attenuated amplitude may develop in viscoelastic media at a stress level below the threshold stress for buckling in an elastic layer and with predicted and observed wavelengths greater than the dominant wavelength. Numerical models using viscoelastic layer in a viscoelastic matrix have been run by Zhang et al. (2000), restricting study to cases in which the viscous and elastic dominant wavelengths are the same. As for a viscoelastic layer in viscous matrix case, there is a transition from viscous properties controlling buckling to elastic properties controlling buckling with increasing strain rate, for a given set of viscous and elastic parameters (Zhang et al., 2000). In one example studied by Mancktelow (1999) and Zhang et al. (2000) the initial layer configuration was in the form of a sinusoidal perturbation with wavelength less than that of the theoretical dominant wavelength for the cases $\mu_L/\mu_M = E_L/E_M = 20, 50, 100$, and 200. At low strain rates the input waveform amplified at a rate consistent with viscous theory, but without the development of the dominant wavelength. At high strain rates, elastic effects became dominant and folds at close to the dominant wavelength developed, replacing the imposed initial waveform, although this change in wavelength does not occur if the initial waveform is perfectly sinusoidal and symmetry is maintained at the model boundaries – in other words in such a case the folds that develop are metastable (Zhang et al., 2000). Slow strain rates led to localized growth of folds from a single isolated initial perturbation, as expected for a viscous layer and matrix, whereas fast strain rates led to the development of periodic folds along the layer, with little difference in amplitude or wavelength between the fold sited on the initial perturbation and the rest of the folds in the train (Fig. 11).

The extent to which elastic properties are significant in folding under natural conditions is unclear. For small folds in competent layers in quartz or calcite veins in slates or schists or quartz-feldspar veins in granitic rocks, which are common in the internal parts of orogenic belts, deformed at typical rates of 10^{-14} s^{-1}, it seems that viscous properties will control fold growth. The value of the strain rate employed in the models of Mancktelow (1999) and Zhang et al. (1996, 2000) that resulted in elastic control of buckling was 10^{-10} s^{-1}. Such a high value may occur locally, such as in narrow shear zones, but it is unlikely to be met in most parts of orogenic belts where most natural folds develop. It should be added, however, that high values of μ_L/μ_M also favour an elastic response to buckling

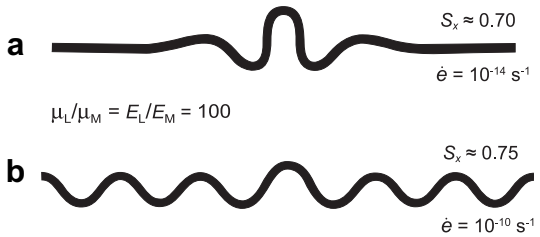

Fig. 11. Numerical models of single layer folds in viscoelastic media developed from an isolated perturbation to show the effect of strain rate on fold development. Initial configuration and rheological properties the same for the two models. E_L = 3.5e11, Poisson's ratio = 0.25, μ_L = 2e21, Deborah number = $\mu\dot{e}/G$ = 0.00007 for top case and 0.7 for lower case for both layer and matrix (Zhang et al., 2000, Fig. 7).

(Schmalholz and Podladchikov (1999), Fig. 2b), and conditions that would most likely lead to an elastic response to buckling would therefore be a combination of fast strain rate and high μ_L/μ_M.

In numerical models where the competent layer is strongly non-linear or plastic, the tendency is for fold growth to be localized and the lateral propagation of folds away from the initial perturbation is reduced (Zhang et al., 1996, Fig. 6; Mancktelow, 1999, Fig. 11). A fuller discussion of analog and numerical modeling of folds with non-linear and power-law rheology, and the rheological effects on fold growth and geometry, will be addressed in subsequent sections.

Anisotropy is an important property of many rocks and, considering the common occurrence of folds in quartz/calcite/feldspar veins in schists, anisotropy in the matrix is probably much more important than anisotropy in the stiff layer in influencing the buckling instability. A characteristic of folding in this situation is that the folds do not die out quickly away from the stiff layer, as they do in an isotropic matrix, but rather propagate well into the matrix (Kocher et al., 2006, 2008). Numerical models show that in a Newtonian matrix the folds maintain a uniform fold form of chevron style, whereas in a power-law matrix the fold form changes and the style is a mixture of kink and chevron (Fig. 12).

2.4. Multilayer folding: theory and modeling

Theoretical treatments of multilayer folding follow generally a similar approach to those for single layers, except that in this case multiple interfaces and layers of several different viscosities are involved (Biot, 1961; Currie et al., 1962; Ramberg, 1964, 1970; Johnson and Fletcher, 1994). Many different configurations have been considered, but it is useful to consider several particular types, which are illustrated in Fig. 13 (with some natural examples shown in Fig. 2). If several stiff layers of a given viscosity and constant thickness are separated by layers of low viscosity, the response of

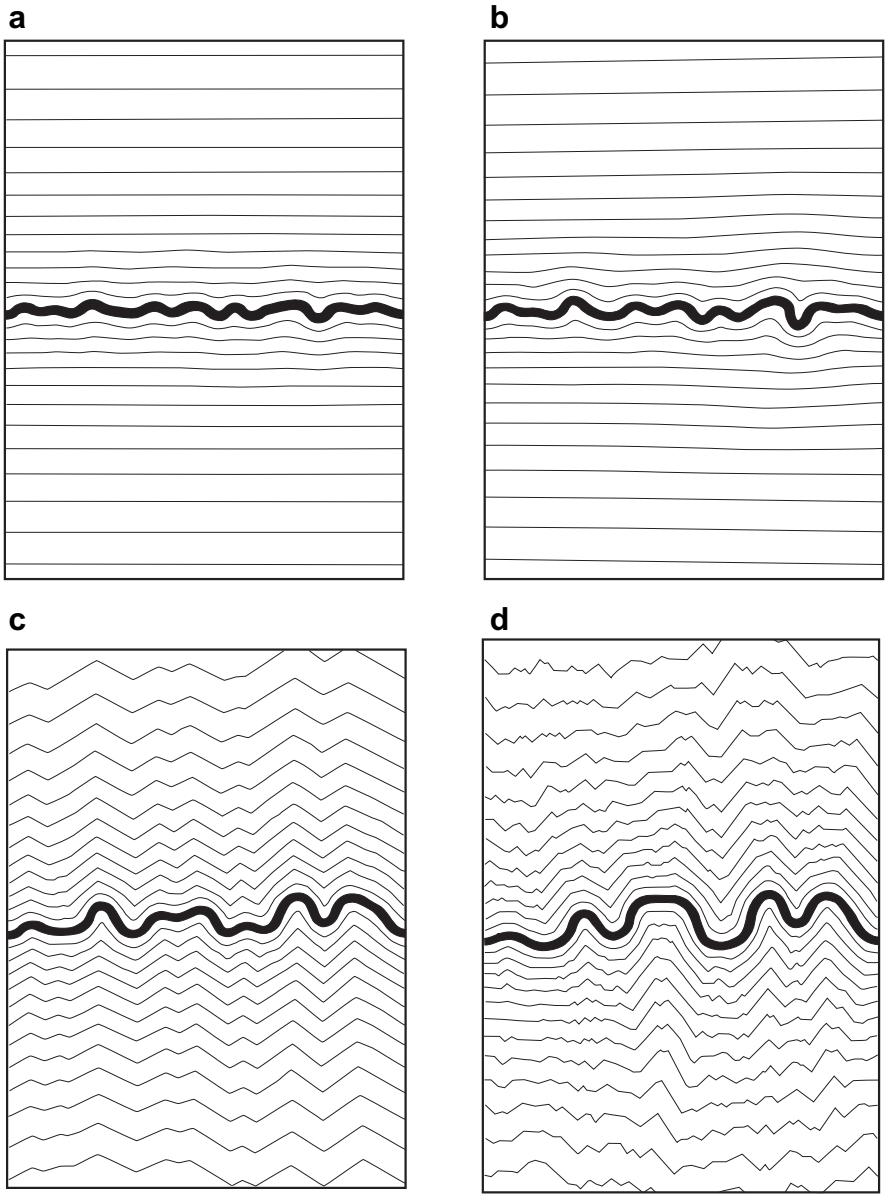

Fig. 12. Numerical models of folding of a single Newtonian layer embedded in a matrix of various properties (Kocher et al., 2006). The same initial random layer irregularities (red noise) and the same ratio of normal viscosity of layer to normal viscosity of matrix, $\mu_L/\mu_M = 50$, in all cases. All shortened by 40%. (a) Linear isotropic viscous matrix; (b) isotropic power law ($n_M = 3$) viscous matrix; (c) anisotropic ($\delta_M = 6$) linear viscous matrix; (d) anisotropic ($\delta_M = 6$) power-law ($n_L = 3$) viscous matrix.

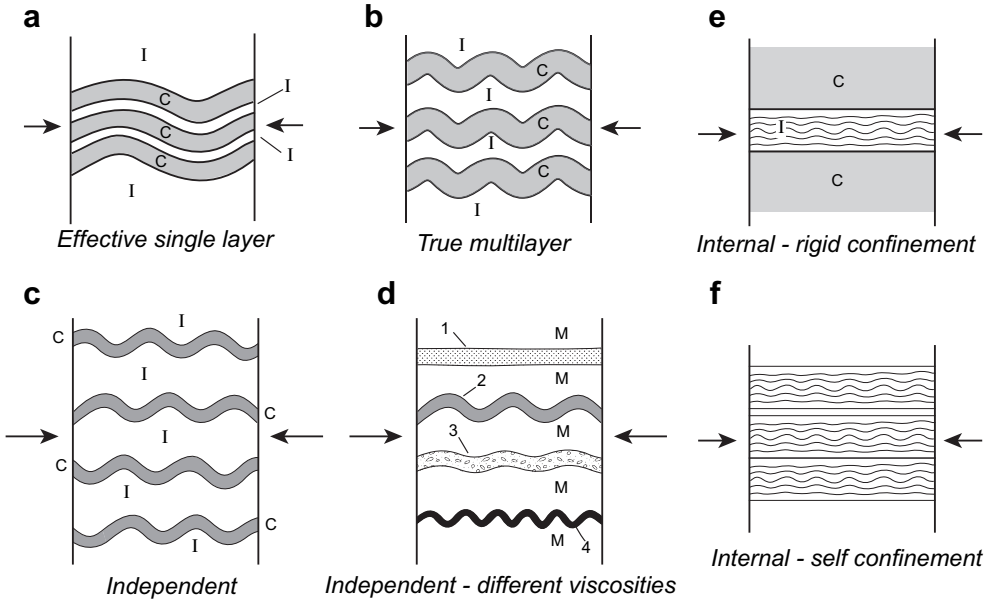

Fig. 13. Idealized configurations of multilayer buckling. (a) Package behaves as an effectively anisotropic single layer. (b) Buckling instability in individual layers coupled to those of neighbors ("true multilayer" of Schmid and Podladchikov, 2006). (c) Stiff layers of the same composition folding independently of neighbors. (d) Fold wavelength of individual layers determined by local viscosity contrast, $\mu_4 > \mu_2 > \mu_3 > \mu_1 > \mu_M$ (after Ramberg, 1964). (e) Internal buckling of laminated medium, equivalent to an anisotropic layer sandwiched between two stiff layers (after Biot, 1964). (f) Internal buckling of laminated medium equivalent to an anisotropic self-confined medium (after Biot, 1965c).

the system depends on the number and spacing of the stiff layers as well as the viscosity contrast between the stiff layers and the matrix. If a multilayer of thickness H, embedded in an infinite matrix of viscosity μ_M and consisting of alternating stiffer and softer layers of viscosity μ_1 and μ_2 occupying fractions α_1 and α_2 of the total thickness, it can be considered an effectively anisotropic single layer, with normal and shear viscosities, μ_n and μ_s given by:

$$\mu_n = \alpha_1\mu_1 + \alpha_2\mu_2, \quad \mu_s = \frac{\mu_1\mu_2}{\alpha_1\mu_2 + \alpha_2\mu_1}, \tag{10}$$

If $\mu_M/\mu_s << 0.2(\mu_s/\mu_n)^{1/2}$, a relationship for the dominant wavelength identical to Eq. (1) can be derived (Biot, 1965b), if h is replaced by H and μ_L by μ_n in equation (1).

$$\frac{\lambda_d}{H} = 2\pi\left(\frac{\mu_n}{6\mu_M}\right)^{1/3}. \tag{11}$$

It corresponds to the situation shown in Fig. 13a. Biot called this *similar folding of the first kind*, although this is not a similar (Class 2) fold according to the standard geometric classification (Ramsay, 1967, p. 367), but rather a parallel fold (Class 1B).

If $\mu_M/\mu_s >> 0.2(\mu_s/\mu_n)^{1/2}$, the bending resistance of the individual stiff layers in the multilayer becomes significant, and the response of the multilayer corresponds to the situation in Fig. 13b. The dominant wavelength is given by:

$$\frac{\lambda_d}{h_1} = 2\pi\left(\frac{N\mu_L}{6\mu_M}\right)^{1/3}, \tag{12}$$

where h_1 is the thickness of the stiff layers within the multilayer and N the number of stiff layers. Biot called this *similar folding of the second kind,* and in this case the overall geometry of the folds is similar (Class 2), achieved by alternating Class 1B and Class 3 geometries of the stiff and soft layers.

The above expressions for dominant wavelength are derived from thin plate analysis (Biot, 1961, 1965b). If shear stresses between layers are significant or if there are intervening soft layers, thin-plate theory is inadequate. Johnson and Fletcher (1994) carried out a thick plate analysis of multilayer folding for a system consisting of layers of arbitrary thicknesses and viscosities that allows accurate calculation of growth rates and dominant wavelengths by an iterative process. Depending on the layer configuration, this may result in growth rate spectra with more than one maximum, which is the situation investigated to find conditions that may result in *parasitic folding* (Ramberg, 1963, 1970; Johnson and Fletcher, 1994, chapter 6; Frehner and Schmalholz, 2006; Treagus and Fletcher, 2009) discussed below. For any particular configuration, change of the preferred wavelength with shortening can be found as for single layers (see Eqs. (7), (8)), and is expressed for multilayers, as for single layers, by an expression equivalent to Eq. (5) (Johnson and Fletcher, 1994, p. 312).

As spacing between stiff (competent) layers is increased, in a simple package with stiff layers of equal thickness and spacing, there is a transition from effective single layer behavior (Fig. 13a) to what Schmid and Podladchikov (2006) call "true multilayer" behavior (Fig. 13b) and then a transition to single layer behavior, in which the layers fold independently (Fig. 13c, and a natural example in Fig. 2a). As the spacing is progressively increased, growth rates increase over what is predicted by the Biot theory for a single layer, reaching a maximum when the alternating stiff and soft layers have equal thickness (Fig. 14), which corresponds to true multilayer behavior (Fig. 13b). Growth rates also increase as the number of layers is increased, but tend towards a 'saturation' value that depends on viscosity ratio (Schmid and Podladchikov, 2006, Fig. 5). As argued by Ramberg (1960, 1961), the key to determining whether the package behaves as a true multilayer or as independent single layers is the spacing in relation to the dominant wavelength. When spacing is greater than the single layer dominant wavelength, λ_d, a distance that Ramberg called the zone of contact strain, the individual layers in the package behave independently. Schmid and Podladchikov (2006) argue in a reciprocal sense that when the spacing is less than $1/\lambda_d$ the package behaves as an effective single layer. These distances correlate fairly well with the ends of the central plateau in Fig. 14a.

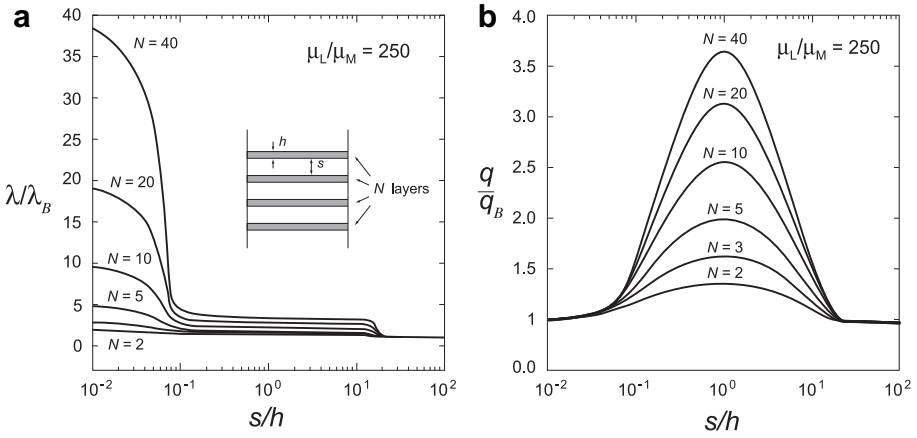

Fig. 14. Theoretical dominant wavelengths (a) and corresponding growth rates (b) for folds in individual layers in a multilayer package consisting of N stiff layers of viscosity μ_L, thickness h and spacing s separated by layers of viscosity, μ_M, with the whole package embedded in two half spaces of viscosity, $\mu_M \cdot \mu_L/\mu_M = 250$. Growth rates and wavelengths are normalized against the Biot thin-plate values (from Schmid and Podladchikov, 2006, Fig. 3).

Treagus and Fletcher (2009) examined *scales of folding in multilayers*, specifically asking why small-scale folds initiate in multilayers, when it is known from theory and modeling (Biot, 1961, 1965a; Ramberg, 1963, 1964; Johnson and Fletcher, 1994; Mühlhaus et al., 2002; Schmid and Podladchikov, 2006), that a multilayer comprising numerous stiff layers will fold with a stronger amplification than a single stiff layer in the same host and that buckling instability increases with the number of stiff layers. Using analytical mechanical models, Treagus and Fletcher (2009) investigate the conditions where small folds of one or two layers might initiate with a strong enough instability to become small-scale 'minor' folds preserved around the larger-scale folds. They find that small folds in one layer are likely to outgrow larger multilayered folds (a) if the thin layer is the stiffest of all the layers, or (b) if the multilayer is narrowly or stiffly confined. Fig. 15 illustrates the process, and the progressive change from initially symmetric to asymmetric minor folds around a major fold with progressive deformation. Frehner and Schmalholz (2006) provide another model whereby minor folds develop and grow more quickly than major folds; here, the important mechanism is that the initial layer irregularities play a more significant part in fold initiation and growth, the thinner the layer.

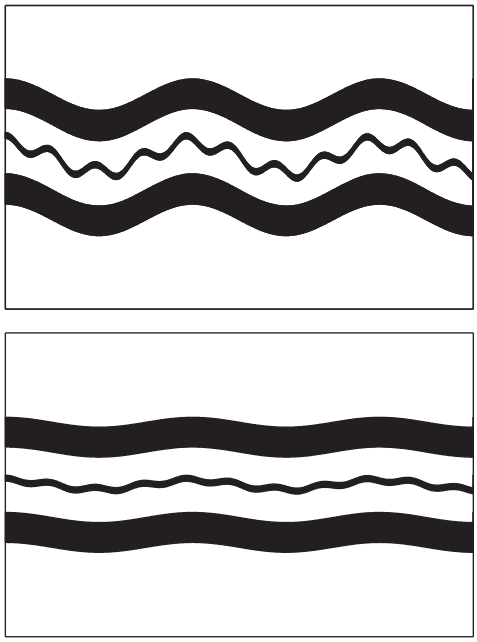

Fig. 15. Model results of the development of asymmetry in minor folds around a larger-scale multilayer fold, where the central thin layer is twice the stiffness of the outer, thicker, stiff layers. The viscosity ratios of dark layers to matrix are 20 and 40. From Treagus and Fletcher (2009).

The configuration shown in Fig. 13e in which folding develops in a multilayer sandwiched between two very stiff and unfolded layers was termed *internal buckling* by Biot (1964, 1965a,b,c). A comparable pattern of folding may develop in an infinite multilayer, which Biot (1965c) has termed self confinement (Fig. 13f, with a natural example shown in Fig. 2c). In these cases the wavelength is given by the empirical relation (Biot, 1965c):

$$\lambda_d = 1.90\left(1 + 3.63\frac{\mu_1\alpha_2}{\mu_2 m}\right)^{1/6}\sqrt{h_1 H}, \tag{13}$$

where the multilayer consists of N alternating layers of viscosity μ_1 and μ_2 and thicknesses h_1 and h_2, with $h_1 + h_2 = 2h$ and $\alpha_2 = h_2/2h$ and $\mu_1 > \mu_2$. The total thickness of the package or wavelength in the y direction in the case of self confinement is, $H = Nh$. If the soft layer is vanishingly thin, $\alpha_2 = 0$ and

$$\lambda_d = 1.90\sqrt{h_1 H}. \tag{14}$$

This holds only if there is sufficient lubrication retained at the interfaces of the layers. This expression also holds approximately for a multilayer with stiff and soft layers of equal thickness when $\mu_1/\mu_2 < 1000$ (see Biot, 1964, Fig. 4).

An analysis of folding has also been carried out for homogeneous anisotropic materials, in which discrete layers do not exist. This corresponds to the conditions required for folding in foliated rock. Cobbold (1976a, 1976b) showed that symmetric sinusoidal similar folds of low amplitude in linear viscous anisotropic media will grow into high amplitude chevron folds if the anisotropy is large, and Casey and Huggenberger (1985) extended this approach to treat asymmetric folds in a non-coaxial strain history. Fletcher (2005) analyzed the instability and development of cylindrical structures in a power-law anisotropic medium, equivalent to a foliated rock. He demonstrated the existence of band-like instabilities whose orientation depends on the ratio of foliation-parallel extension to foliation-parallel shear, but there is no characteristic λ/h as there are no layers to give a definition to thickness. Fletcher's results (Fletcher, 2005, Fig. 5) include structures that are equivalent to the self confinement of Biot (1965a).

Internal buckling in multilayered and/or anisotropic media, and the spectrum of folding styles from chevron folds to kink bands, have been demonstrated in analog models by Ghosh (1968), Cobbold et al. (1971) and Latham (1979). Latham (1985a,b) investigated relationships across the spectrum of folding, kinking and faulting, in anisotropic non-linear materials in theory and laboratory experiments. Examples of different configurations of multilayer and resulting differences in fold geometry are shown in Fig. 2.

2.5. Oblique-layer folding, non-plane strain and non-coaxial deformation

Nearly all the theory and modeling of folds, reviewed above, concerns plane strain with layers parallel to the maximum shortening direction and maximum extension perpendicular to the layering. The waveforms considered are cylindrical, developing into folds with axes parallel to the direction of no strain. It has been shown both theoretically (Fletcher, 1991, 1995) and experimentally, in single layers (Grujic and Mancktelow, 1997) and multilayers (Watkinson, 1975), that folds also develop in plane strain with maximum extension of the base flow parallel to the layer (rather than perpendicular to the layer) and with the fold axes parallel to the direction of maximum extension, In this case the growth rates are reduced, increasing the viscosity ratio required to produce significant folding and, for a given viscosity ratio, increasing the amount of layer-parallel shortening that precedes large-amplitude fold growth.

It has been shown (Treagus, 1973) that the same dominant wavelength of a cylindrical waveform as given by Eq. (1) would arise for Newtonian materials under conditions of plane strain but with the layer oblique to the principal compression (but parallel to the direction of intermediate stress and strain). To first order, the initial low-amplitude buckles are symmetric (Treagus, 1973; R.K. Davies and R.C. Fletcher, personal communication, 2009), but become asymmetric during progressive folding, as shown in finite-element models (Anthony and Wickham, 1978). The same principles have been shown to apply to folds that develop in non-coaxial deformation, such as in transpression (James and Watkinson, 1994), provided there is a component of shortening along the layer. Folds in these situations grow perpendicular to the instantaneous maximum shortening direction in the layer.

If the layer has initial sinusoidal waveforms in both x and y directions in the plane of the layer, with wavelengths λ_x and λ_y, and with shortening in both x and y directions, Fletcher (1991) shows that a cylindrical waveform (i.e. $\lambda_y = \infty$) with axis perpendicular to the maximum shortening rate of the basic flow grows most rapidly, although the growth rate is not markedly greater than that when $\lambda_x/\lambda_y > 0$, that is when the folds are non-cylindrical with increasing aspect ratio as λ_x/λ_y increases. This is true for most values of $\dot{e}_x/\dot{e}_y$, but when $\dot{e}_x = \dot{e}_y$ (that is equal shortening rate in both x and y directions) the instability disappears and all fold forms grow at an equal rate. If initial random perturbations in both x and y are amplified, the tendency of the resulting fold form to cylindricity increases with amplification, and is stronger for a power-law layer than a Newtonian layer (Fletcher, 1995). In the power-law case, for a cylindrical perturbation with axis parallel to y, the stress exponent n in the expression for the growth rate must be replaced by an apparent stress exponent, n^*, where:

$$n^* = \frac{4n\left(1+\xi+\xi^2\right)}{4\left(1+\xi+\xi^2\right)+3(n-1)\xi^2}. \quad (15)$$

where ξ is the ratio of the in-plane deformation rates of the basic-state flow, $\dot{e}_y/\dot{e}_x$.

Kaus and Schmalholz (2006) and Schmid et al. (2008) investigate numerically the development of folds to finite amplitude in a three-dimensional strain field, with different rates of shortening in x and y directions in a competent layer with random initial irregularities in x and y. These studies confirm the analytical finding of Fletcher (1991, 1995) that a waveform with axis (y direction) perpendicular to the maximum shortening rate (x direction) grows most rapidly, regardless of the value of the shortening rate in the perpendicular direction and that there is no preferred wavelength in this perpendicular direction. Even so, folds tend to develop with a characteristic aspect ratio, λ_x/λ_y, which depends systematically on the ratio of strain rates in the x and y directions, with aspect ratio, or cylindricity, increasing as strain rate in the y direction changes from negative to positive. Schmid et al. (2008) note that the initial exponential growth rates predicted by theory give way to slower growth rates, controlled by layer length, as occurs in two dimensions (Schmalholz and Podladchikov, 2000) and as modified for three dimensions by Kaus and Schmalholz (2006).

Experiments show that the folds that form under simple shear are, at least for small amplitudes, symmetric (Ghosh, 1966; Manz and Wickham, 1978; Viola and Mancktelow, 2005), as for the inclined layers above. Growth to finite amplitudes, both in terms of growth rate and orientation of the fold axes with respect to the far-field principal strain axes, is complicated by the non-coaxial nature of the deformation (Flinn, 1962; Ghosh, 1966; Treagus and Treagus, 1981). The situation is further complicated for non-Newtonian materials, as the case analyzed exactly by Fletcher (1995) indicates, since the individual stress and strain rate components are related through the second invariant of deviatoric stress, which depends on all three principal stresses. If the principal stress in the third dimension (y say, parallel to the fold axis) dominates the second strain rate invariant, then the invariant will not change much in response to variations of stress component in the xy plane that control fold development. The degree of non-linearity of flow associated with folding and hence growth rates of folds will be diminished. In the situation described by Eq. (15), if the power-law exponent is 3 and the extension in y is equal to the shortening in x, the effective stress exponent, n^*, becomes 1.2, which is only weakly non-linear. This effect will not be large in cases for which the fold axis is parallel to the intermediate bulk strain and thus to a direction of small deviatoric stress.

2.6. Folding of oblique layers in general three dimensional strain fields

Some cases of folds developing in a three-dimensional strain field have been considered in the previous section. If the layering is oblique to all three far-field principal stresses or strain rates, the directions of maximum shortening rate in the competent layer varies continuously with time and the base strain rate on which a buckling instability would be superimposed is therefore also changing. This is true for a bulk coaxial strain history, and true but further complicated for a bulk non-coaxial strain history. Flinn (1962) considered how the finite strain and potential positions of fold hinges vary in layers oblique to the principal strain directions in a bulk coaxial strain field of various strain symmetries. Additional features of folding in 3D will be discussed in 6.4.

3. Information from wavelength/thickness ratios of single-layer folds

Fold theory and modeling, reviewed in Section 2.1–2.6, provide the basis for analysis and interpretation of natural folds and their wavelengths, leading to information about the rheological

properties of rocks. Equations, such as (1), (4), (5) and (6), define dominant or preferred wavelength-thickness ratios for single-layer folds under different rheological and strain conditions. For low-amplitude folding, these equations can be applied to folding of layers that are not parallel to maximum compression, and to deformations other than pure shear, such as simple shear and transpression, with a caveat for non-linear behavior discussed in Section 2.5.

3.1. Wavelength selection

The irregularities in natural layer interfaces may be considered as the sum of the components of a harmonic series. In linear theory the growth rates of folds of different wavelength are linearly independent, and there will be competition among the various harmonic components. It is assumed that the folds that emerge are those of the wavelength with the fastest growth rate, that is the *dominant wavelength* or, in the case in which layer-parallel shortening is significant, those with the wavelength that has the greatest cumulative amplification, that is the *preferred wavelength*. Because, for viscous materials, all harmonic components are amplified, the final waveform will reflect the superposition of the amplification spectrum on the amplitude spectrum of the initial irregularities (Fletcher and Sherwin, 1978) and thus not be truly periodic unless the initial amplitude spectrum is periodic.

The process of wavelength selection, in which a particular wavelength spectrum emerges and becomes locked in, with hinges fixed, must have ceased by the time the crossover amplitude of Schmalholz and Podladchikov (2000), discussed in Section 2.2, is attained. Schmalholz (2006) finds the limb dip at which the crossover amplitude is reached is about 17°, which is in general agreement with earlier studies that noted that most shortening of the layer ceases when folds attain limb dips of 15–20° (Sherwin and Chapple, 1968; Hudleston, 1973a). Schmalholz (2006) shows that if amplitudes are scaled to the crossover amplitude, all plots for the change in amplitude with strain fall on essentially the same curve (Fig. 16). An additional stage of folding, beyond the point where the crossover amplitude is exceeded, can be identified when the growth rate decreases to zero, or in fact becomes slightly negative (Fig. 16). During this stage the growth is essentially kinematic, although this is only approximately so because the arclength of the fold is essentially constant, whereas in true kinematic behavior the local change in arclength will depend on position around the fold – shortening in the hinge and extension in the limbs if the limb dips are greater than 45°.

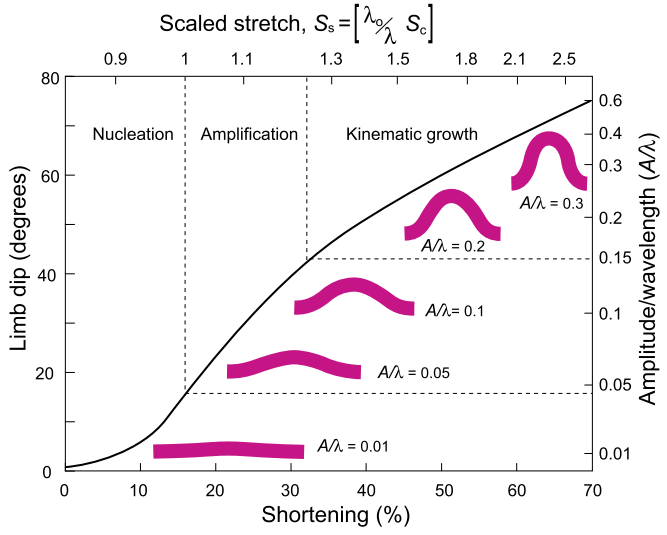

Fig. 16. Scaled amplification curve (Schmalholz, 2006, Fig. 3), plotting limb dip or amplitude/wavelength against shortening. The black line is calculated for $q_o = 15$ (corresponding to a viscosity contrast of about 50) and $A_o/\lambda_o = 3e{-}3$ (corresponding to a limb dip at the inflexion point of about 1°). The fold shapes are numerically simulated single-layer folds for a viscosity contrast of 50. The crossover stretch, S_c, is given by Schmalholz (2006, Eq. (8)).

Natural and experimentally produced folds show a range in values of wavelength/thickness or arclength/thickness. If fold trains are divided up into segments bounded by hinges and/or inflexion points, the distance between adjacent hinges is a measure of half wavelength, or the distance between inflexion point and hinge a measure of a quarter wavelength (Fig. 17a). Using such a measure, Schmalholz (2006) shows that the growth of each individual fold in a quasi-periodic fold train developed from a layer with random initial perturbations follows the normalized amplification curve. Based on the observation that little change in arclength occurs for folds with limb dips >15–20°, it has been suggested that the arclength of mature folds provides a good measure of wavelength at the time that wavelength selection ceases (Fig. 4, Hudleston, 1973b, 1986; Fletcher and Sherwin, 1978). Frequency distributions of wavelength/thickness for natural folds (Fig. 17b) are similar in form to amplification spectra, as pointed out by Sherwin and Chapple (1968), leading to the suggestion that the mean value of L/h for a natural fold population, $\bar{L}/h$, may be a good measure of the wavelength/thickness of the folds that have received maximum amplification, λ_p/h. This assumption has been used in estimating viscosity contrast in natural folds (Sherwin and Chapple, 1968; Hudleston, 1973b; Hudleston and Holst, 1984). A test of this assumption was made by Fletcher and Sherwin (1978) who showed empirically that this relationship holds provided the initial irregularities in the layer correspond to a spectrum of white roughness, which is arguably a reasonable approximation to many natural surfaces. If, on the other hand, the harmonic components in the initial layer have constant amplitude, $\bar{L}/h$ underestimates λ_p/h, by an amount that can be determined and that depends on the dispersion of the distribution. In addition, Fletcher and Sherwin showed that the dispersion (standard deviation/mean) of the frequency distribution of L/h is related to the relative bandwidth of the amplitude spectrum of the harmonics present in the fold shape. The relative bandwidth can then be used to estimate the maximum amplification the folds have undergone.

3.2. Field data and inferences

Data on arclength/thickness, L/h, measured in the way illustrated in Fig. 17a, are shown for a single population of folds in Fig. 17b and for published populations of folds in Table 1. Data of this type have been the subject of recent discussion (Treagus and Hudleston, 2009; and Schmid et al., 2010). Values of L/h in Table 1 range from 2–30, with means from 3.7 to 14.5 for a variety of compositions of both layer and matrix. If the mean value of L/h is taken as the dominant wavelength/thickness, λ_d/h, and the viscosity is assumed to be Newtonian, these values imply a range of viscosity ratios from 2 to 75 applying thin-plate theory and somewhat smaller values applying thick-plate theory. As Sherwin and Chapple (1968) and subsequent experiments and numerical models have shown, these values are so low in most of these examples that significant layer-parallel shortening would have occurred before the amplification could have been sufficient to bring the folds to the stage at which the wavelengths became locked in, that is when the folds attained limb dips of about 15°. Indeed, for the lowest values of L/h and at the lowest apparent viscosity ratios the buckling instability would have been masked by kinematic amplification.

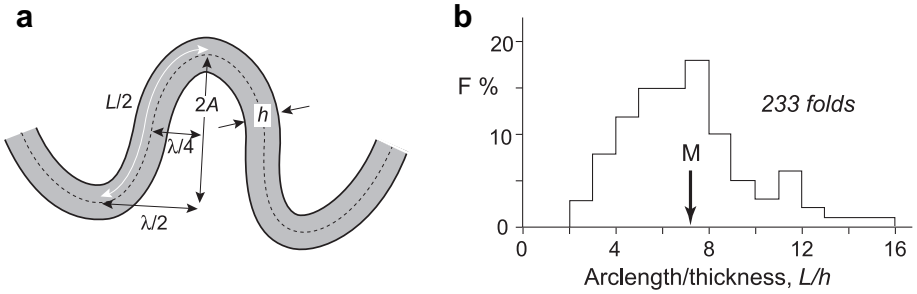

Fig. 17. (a) Local measures of fold amplitude, *A*, thickness, *h*, wavelength, λ, and arclength, *L*, for quasi-periodic folds as typically found in nature. These were the measurements used to produce the histogram in (b) for folds in calcite veins and limestone beds in slates east of Golden, British Columbia (after Hudleston, 1986). M indicates the mean.

If the mean value of L/h is taken as the preferred wavelength/thickness, λ_p/h, as is appropriate for an initial distribution of irregularities in the form of white roughness (Fletcher and Sherwin, 1978), to attain an appropriate degree of amplification, in the range 10–100 (Sherwin and Chapple, 1968; Fletcher, 1974; Hudleston and Holst, 1984; Schmid et al., 2010), implies large amounts of shortening if Newtonian viscosity is assumed. All the studies (except Holst, 1987) for which strain data are available in Table 1 indicate limited amounts of shortening, the maximum being $T = 1.5$ (or shortening of the layer of about 20%), but with likely values being much less than this. The required amounts of shortening are significantly reduced if power-law behavior is assumed, which leads to higher amplification rates at smaller values of λ_d/h and λ_p/h (as indicated by Fig. 6).

Because of the lack of good knowledge of the initial form and amplitude of initial layer irregularities, the limited information available on the early layer-parallel shortening of folded layers, and the possibility of rheological behavior not properly accounted for in the theoretical models used in the analysis, it is not possible to make precise estimates of viscosity contrasts and power-law exponents from the kind of data presented in Table 1. However, useful information can be obtained from analysis of natural fold populations. As an example, using the data of Hudleston and Holst (1984), and Fletcher's thick plate theory, if we take the mean $L/h = 6.5$ to be L_p/h and the amplification required to lock in this wavelength as 20, assuming a power-law exponent $n = 1$ for layer and matrix (i.e. Newtonian) implies a viscosity ratio of 17 and an initial layer-parallel shortening of about 35%. The viscosity ratio is reasonable, but the measured shortening is probably less than 5% and certainly less than 20%. Increasing the amplification worsens the problem and reducing it to 5 still requires excessive shortening (Hudleston and Holst, 1984). If we take a power-law exponent $n = 3$ for layer and matrix, with the same amplification, it implies a viscosity ratio of about 17 and a shortening of 18%, which is within the range of estimates of measured strain. Applying different analytical solutions to natural single-layer folds, Schmalholz and Mancktelow (2008) estimated the viscosity ratio to lie in the range 20–70 and the power-law exponent of the layer to lie between 1.8 and 5.

A tentative conclusion from the above, and also from the discussion of Schmid et al. (2010), is that the measured single-layers folds in the rocks shown in Table 1, more closely approximate to power-law rheology than to Newtonian or viscoelastic rheology. However, it should be pointed out that these data sets of fold wavelengths mostly concern folded veins of quartz, calcite or pegmatite, on the scale of mm to cm. There is very little evidence on

Table 1
Arclength/thickness data for single-layer folds.

Mean L/h	Range	Number of folds	Strain in profile plane, T	Stiff Layer	Matrix	Source
5.5	2–14	473		quartz veins	phyllite	Sherwin and Chapple (1968)
4.5	2–13	142		quartz veins	sandy	Sherwin and Chapple (1968)
5.2		582		quartz veins	slate	Sherwin and Chapple (1968)
6.8		9		quartzite	slate	Sherwin and Chapple (1968)
5.1		83		quartz veins	slate	Sherwin and Chapple (1968)
4.0		12		siltstone	slate	Sherwin and Chapple (1968)
5.7		17		quartzite	phyllite	Sherwin and Chapple (1968)
3.7	1.5–8	157		quartzo-feldspathic veins	pelitic schist	Hudleston (1973b)
6.5		29	1.0–1.5	calcite veins	slate	Hudleston and Holst (1984)
7.0	2–16	233		calcite veins	slate	Hudleston (1986)
9.4	–	3	1.07–1.27	limestone	shale	Fletcher (1974)
[a]5.5	[e]4–13	22		quartz veins	mafic schist	Shimamoto and Hara (1976)
[b]8.0	[e]4–22	52	c. 1.15–1.35	quartz veins	psammitic schist	Shimamoto and Hara (1976)
[c]8.5	[e]5–29	59	c. 1.15–1.35	quartz veins	psammitic schist	Shimamoto and Hara (1976)
[d]14.5	[e]10–25	22	c. 1.06–1.20	quartz veins	pelitic schist	Shimamoto and Hara (1976)
9.2		35		pegmatite	granite	Ramsay and Huber (1987)
6.2	1.5–17.5	343	2.8–4	quartz layers	slate	Holst (1987)
7.8	4.8–11.3	4		quartz veins	calcarenite	Johnson and Fletcher (1994)
12				calc-silicate layer	calcite marble	Schmid et al. (2010)
6.9				quartz-feldspar pegmatite	calcite marble	Schmid et al. (2010)
5.9				quartz-feldspar pegmatite	felsic gneiss	Schmid et al. (2010)

[a] These values are modes, not means, and for a subset of the data that includes only folds with limb dips of 75–90°. The mode of this subset will be closer to the mean of the total fold population than the mean of the subset.
[b] Same as above, for a subset with limb dips of 40–55°.
[c] Same as above, for a subset with limb dips of 15–30°.
[d] Same as above, for a subset with limb dips of 50–60°.
[e] These exclude folds outside indicated ranges of limb dips.

a larger scale, or for a wider range of metasedimentary rock of siliciclastic type, in part because true single-layer folds are uncommon in stratigraphic sequences, especially in the first stage of deformation. Multilayer folding is most commonly seen, and here the wavelength-thickness relationships are harder to analyze. We can find no convincing evidence, to date, to indicate that a wide range of common rocks, such as interbedded quartzites, psammites, and pelites, have folded as power-law multilayers. Indeed, it has been argued from other structures such as cleavage refraction and conglomerate deformation that suggest quite small viscosity contrasts in rocks (Treagus, 1999; Treagus and Treagus, 2002; Czeck et al., 2009), that under these conditions of deformation, the rocks might be considered approximately Newtonian.

It should be possible to identify buckle folds that develop in single layers within an anisotropic matrix by the propagation of folds away from the layer well into the matrix, as shown in the numerical models of Kocher et al. (2006) (Fig. 12). Getting information on viscosity contrast will be more difficult than for single layers in an isotropic matrix because yet another parameter, the anisotropy factor, δ, is introduced.

Despite the uncertainties discussed above, it should be possible for some populations of folds, and using information discussed below in sections 4 and 5, in addition to wavelength/thickness data, to define with more precision the parameter space in which natural folds lie. For multilayer folds, the eigenvalue/eigenvector method of Johnson and Fletcher (1994) offers the possibility of modeling specific layer configurations to match natural examples, although again the number of parameters to consider makes this a challenge.

4. Information from fold shapes

Fold shapes in rocks are highly variable, especially in multilayers (e.g. the illustrations in Weiss, 1972; Price and Cosgrove, 1990, chapters. 12, 13; Hudleston and Lan, 1993; Fig. 2). This reflects differences in the mechanical response due to differences in layer thickness, viscosity, degree of anisotropy, deformation intensity and deformation path, as well as the influence of initial layer irregularities. Many methods have been proposed for characterizing fold shape, on the basis of thickness variations (e.g. Ramsay, 1967, p. 360; Lisle, 1997), dip isogons (Ramsay, 1967, p. 363; Hudleston, 1973c), relationships among selected fold parameters – including amplitude, wavelength, interlimb angle, hinge curvature (e.g. Twiss, 1988) – and by utilizing various mathematical functions, including harmonic functions (e.g. Stabler, 1968; Hudleston, 1973c), power functions (Bastida et al., 1999), conic sections (Bastida et al., 2005), and Bezier curves (Srivastava and Lisle, 2004). We do not attempt to review all these here, but refer readers to the review by Bastida et al. (2005).

4.1. Single layers

The most regular and reproducible shapes are found in folds that approach periodic form with a single wavelength, both in nature (Fig. 1a,b) and in analog or numerical models (Fig. 10). By contrast, when different wavelengths of comparable amplitude are represented in finite amplitude folds – which is most likely to occur when the initial irregularities are large and the selectivity of the folding poor–the shapes are less regular (e.g. the right hand side of Fig. 10). Periodic buckle folds are initiated with close to sinusoidal form and these grow to become more rounded in the hinge than sinusoidal, unless the layer rheology is strongly non-linear (Chapple, 1968), strongly anisotropic (Lan and Hudleston, 1996), strain softens (Neurath and Smith, 1982), or fracturing occurs (Tentler, 2001) in the hinge, in which case the fold shape can become quite angular. The change in shape with fold growth can be quantified by employing harmonic analysis (Hudleston, 1973c), power functions (Bastida et al., 1999) or other means (Bastida et al., 2005). The departure from sinusoidal shape is predicted by third order buckling theory (Johnson and Fletcher, 1994) and is clearly seen in analog and numerical models (e.g., the succession of fold shapes in Fig. 16; Hudleston, 1973a).

Schmalholz and Podladchikov (2000) found that the first two terms of the Taylor series that can be employed to define the arclength of a sine function, strictly applicable only for small values of A/λ, match the arclengths of numerically produced single layer folds up to limb dips of about 50°. The shape of the folds, as distinct from arclength, also starts to deviate significantly from sinusoidal at about 50° limb dip. Also, as amplitude increases, fold shape increasingly becomes sensitive to non-linearity in the flow law. As the power-law exponent of the stiff layer increases, folds tend to be sharper hinged and longer limbed, a change associated with deformation tending to become localized in the hinge region. This can be noted by eye if folds of similar arclength/thickness ratio are compared (Fig. 18) and quantified if some appropriate measure of shape is used. Numerical models by Hudleston and Lan (1994) showed, by varying λ_o/h_o, μ_L/μ_M, n_L and the shape of the initial layer perturbation, that the main factor controlling sharpness of fold hinges is n_L. They employed a curvature index, *Ki* (see Fig. 18, inset), that varies between 0 for a fold represented by a circular arc, 1 for a chevron fold, and 0.75 for a sine function with limb dip of 45°. The biggest shape difference among folds in layers with

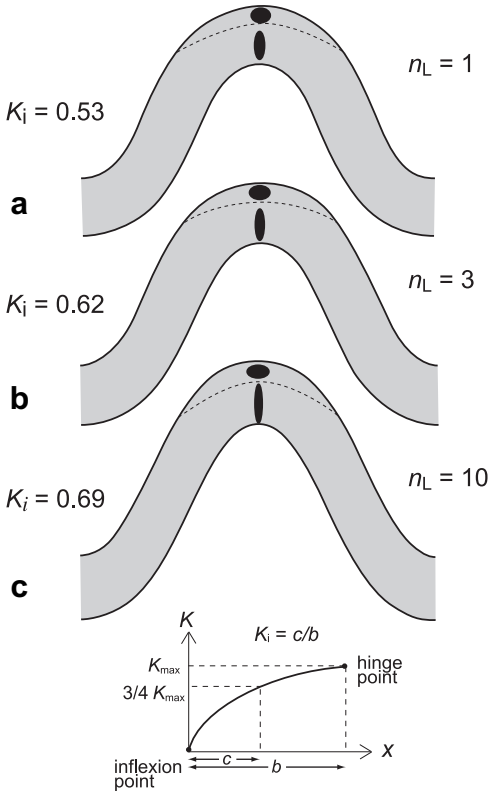

Fig. 18. Numerical models of single-layer folds in a power-law stiff layer embedded in a Newtonian matrix, with base viscosity contrast $\mu_L/\mu_M = 100$, developed from an identical starting sinusoidal shape with $L_o/h_o = 12$ and $A_o/h_o = 0.1$. Three cases shown for $n_L = 1$, 3 and 10, all at 50% bulk shortening. Also shown are the sharpness parameter, *Ki*, and schematically the strain in the inner and outer arcs of the fold, separated by a dashed line representing the finite neutral surface. The inset shows how curvature index is defined for a fold segment between hinge and inflexion point (see also Hudleston and Lan, 1994). *K* is curvature. The value of *Ki* for a sine function with the same limb dip (about 63°) for these folds is 0.86.

different power-law exponents is for wavelengths greater than about 10 and at limb dips of 40–70 (Fig. 18). If the shapes of folds at a given limb dip are compared, hinge sharpness, as measured by *K*i, increases with *L*/*h* with little dependence on n_L, until values of about *L*/*h* ≈ 10 are attained (Fig. 19). For values of *L*/*h* greater than about 10, hinge sharpness changes little with increase in *L*/*h*, but there is a clear increase in sharpness as n_L is increased. An alterative plot of hinge sharpness at a given value of *L*/*h* (with *L*/*h* > 10) gives similar results and shows that hinge sharpness increases only slowly with limb dip (Fig. 20). This dependence of hinge sharpness on non-linearity of flow behavior in the stiff layer is expected and consistent with Chapple's (1968) theoretical results of folding a viscous-plastic beam in which plastic failure occurs in the hinge.

In principle, hinge sharpness can be used to gain some information about rheological properties from natural folds (Hudleston and Lan, 1993). Data for a set of minor folds in siltstone layers in shale from the Appalachians are included in the plots in Figs. 19 and 20. The data cluster above the line representing $n_L = 3$, with many points above the line for $n_L = 10$. This suggests highly non-linear rheological behavior, although, as discussed below, other factors can also lead to sharp-hinged folds. It is clear from

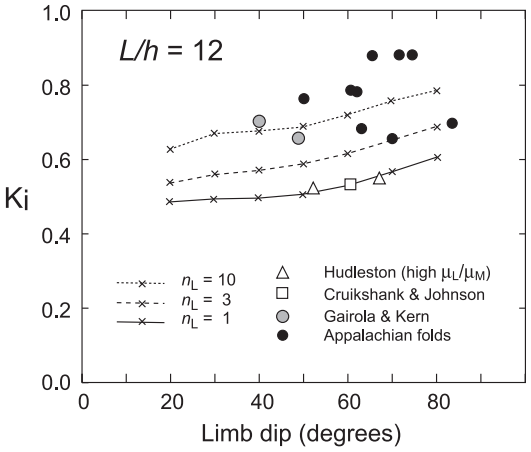

Fig. 20. Sharpness parameter, *K*i, as a function of limb dip at fixed arclength/thickness ratio, *L*/*h* ≈ 12, for numerical (solid lines) and natural and analog (symbols) folds. Data from Gairola and Kern (1984) are for experimentally-produced folds in limestone. Otherwise as in Fig. 19. From Lan and Hudleston (1995a).

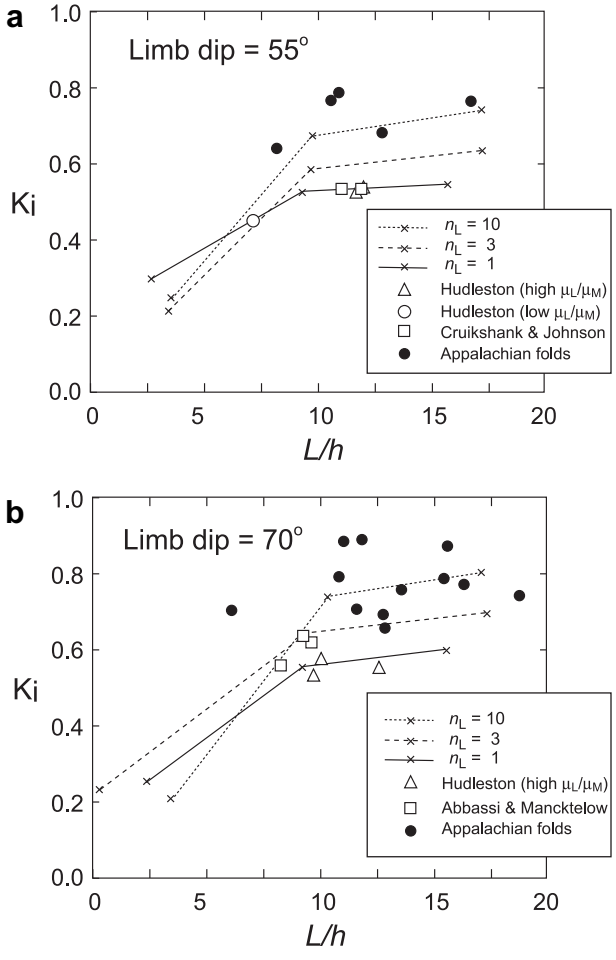

Fig. 19. Sharpness parameter, *K*i, as a function of arclength/thickness, *L*/*h*, at fixed limb dip (55°) for numerical (small crosses joined by solid lines) and natural and analog (symbols) folds: (a) at a limb dip of 55°; (b) at a limb dip of 70°. Selected data for analog models are from Hudleston (1973a,b,c) and Abbassi and Mancktelow (1999); also data for Cruikshank and Johnson's (1993) numerical model. Solid line data are interpolated from results of numerical models with L_o/h_o values of 6–30, $n_L = 1$, 3, 10 and $\mu_L/\mu_M = 100$. Appalachian data are for folds in siltstones in shales. From Lan and Hudleston (1995a).

numerical simulations that random irregularities in the initial layer lead to fold trains with considerable variation in the shapes of individual folds (Fig. 10, Schmalholz and Podladchikov, 2001, Fig. 8, 11; Schmalholz, 2006, Fig. 5; Mancktelow, 2001, Fig. 7). Schmalholz (2006), however, shows that individual folds of different amplitude and somewhat different shape in a fold train follow almost identical scaled amplification curves. This demonstration and the results of Hudleston and Lan (1994) support the proposition that the folds in a fold train that have single well-defined hinges but vary in amplitude and *L*/*h* should have values of relative hinge curvature that reflect the stage of fold growth and the degree of non-linearity in the flow law. A limitation of using relative curvature to identify non-linear rheological behavior is that a value of *L*/*h* = 10 lies towards the upper end of the range of mean values reported for studied natural fold trains (see Table 1). The folds used in shape analysis, however, do not have to be ones corresponding to the dominant (or preferred) wavelength and many natural fold populations, even those with low mean values of *L*/*h*, contain folds with *L*/*h* ≥ 10.

Another factor influencing the sharpness of folds is anisotropy. Fig. 21 compares fold shapes in single layers in which both layer and matrix are anisotropic, with different degrees of anisotropy, δ. It should be possible to identify situations in which anisotropy has influenced folding by the fabric (layer-parallel cleavage or schistosity) in the rocks and by the development of layer-parallel shear strain in the limbs of the fold; such strain being minimal in isotropic layers. This can be seen by comparing the deflection of layer normal markers in Fig. 22a and b. Effective layer anisotropy can also be achieved by alternating stiff and soft isotropic layers within an isolated layer package that may behave as a composite single layer during buckling (Fig. 22c). Sharp-hinged folds of similar shape (measured by curvature index, *K*i) and formed in three different ways are compared in Fig. 22. This serves to demonstrate that layer shape alone is not sufficient to distinguish these situations; it should be considered in combination with internal strain distribution and fabric pattern.

It seems unlikely that the effects of elasticity will be manifest in most natural small folds (see Section 2.6), and there is conflicting information on how elastic versus viscous properties affects the regularity of fold trains. In numerical models of Schmalholz and Podladchikov (2001, Fig. 11), there is much greater variation in shape and strain associated with individual folds in layers in which elastic properties influence folding than in purely viscous layers. By

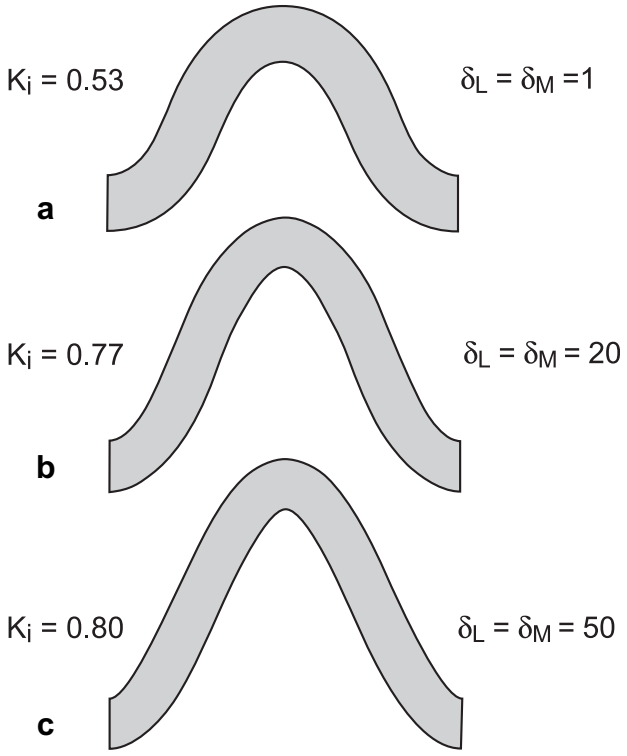

Fig. 21. Numerical models of single-layer buckle folds to show the effect on fold shape of increasing anisotropy, as measured by δ = normal viscosity/shear viscosity. In all cases $L_o/h_o = 12$, $A_o/h_o = 0.1$, $n_L = 1$, $\mu_L/\mu_M = 100$ and bulk shortening = 40%. The value of the curvature index, *Ki*, is shown beside each fold. (a) $\delta_L = \delta_M = 1$ (isotropic layer and matrix), (b,c) $\delta_L = \delta_M = 20$ and 50 (anisotropic layer and matrix). After Lan and Hudleston (1996).

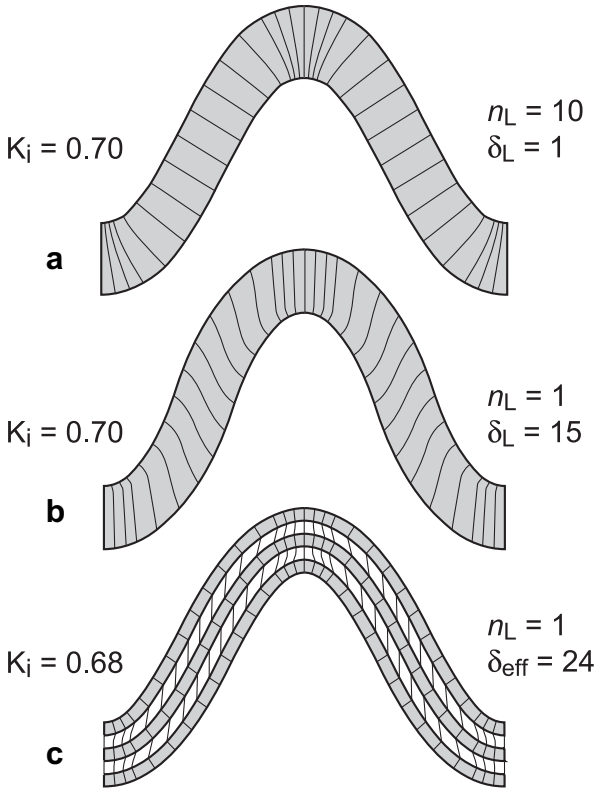

Fig. 22. Numerical models of single layer (a,b) or effective single layer (c) buckle folds of similar values of *L*/*h* and showing similar degrees of angularity (sharp hinges and straight limbs) as measured by shape index, *Ki*, produced by different combinations of rheological conditions. (a) In a highly non-linear isotropic stiff layer with $\delta_L = 1$, $n_L = 10$; (b) in a strongly anisotropic layer with $\delta_L = 15$, $n_L = 1$; (c) in a composite layer consisting of three isotropic stiff layers and two soft layers, with the soft layers the same as the matrix. In all three cases $L_o/h_o = 12$, $A_o/h_o = 0.1$, $\mu_L/\mu_M = 100$ and shortening = 40%. In (c) the effective anisotropy of the package, $\delta_{eff} = 24$, is based on Biot's theory (Biot, 1965a, p. 432–433.). The matrix is Newtonian and isotropic in each case (i.e. $n_M = 1$, $\delta_M = 1$). (Based on Fig. 6 in Lan and Hudleston, 1996). The value of curvature index, *Ki*, is shown beside each fold.

contrast, in models of Zhang et al. (2000), there is more variation in fold shape in layers controlled by viscous properties than in layers in which folds are controlled by the elastic properties. Differences in matrix rheology and choice of elastic and viscous dominant wavelengths likely explain these results.

The shape of buckled layers in 3D – in part the degree of cylindricity of the folds - may contain information about the rheology of single layer folds. Fletcher (1995) showed that the selectivity of buckling for harmonic components with large aspect ratio in *x* and *y* directions in the plane of the layer (with longest dimension perpendicular to the shortening direction) in plane strain depends on the power-law exponent, n_L, such that folds of greater cylindricity will develop from a layer with random perturbations in both *x* and *y* directions in the layer interface for highly non-linear rheology (very large value of n_L, equivalent to plastic behavior) than for Newtonian rheology (Fig. 23). Viscosity contrast also has an effect, with high contrast enhancing cylindricity, but only for non-linear rheology.

Information about folding mechanisms by which the strain in the competent layer is accommodated can be found by applying the techniques of Bobillo-Ares et al. (2004). Fold shapes can be matched by trial and error application of their FoldModeler program (Fig. 24), if information on cleavage orientation around the fold is available and the assumption is made that cleavage reflects the *XY* plane of the strain ellipsoid (with $X \geq Y \geq Z$ being the lengths of the semi axes of the ellipsoid). Unless the value of strain is known at some point in the fold, a full model of fold development cannot be made. This method assumes the processes operating to produce the observed shape and strain are combinations of flexural flow, tangential longitudinal strain and homogeneous flattening.

4.2. Multilayers

Fold shape is much more variable in multilayers than in single layers (e.g. Fig. 2). Characteristic shapes include sinusoidal, chevron, kinks – with axial surfaces inclined to the average orientation of the layering – and conjugate (or box) folds. Straight-limbed folds, either of chevron or kink style, imply effective anisotropy, but do not require discrete layers (as in the case of kink bands in slate) or brittle failure in the hinges. Chevron folds (Fig. 2d) can develop in several ways: from initial sinusoidal shapes (e.g. Johnson, 1977), by the appression of conjugate folds (see Price and Cosgrove, 1990, Fig. 13.45) or by the intersection of kink bands (Paterson and Weiss, 1966; Cobbold et al., 1971). For symmetric folds, a chevron style is inherently favored by anisotropy (Bayly, 1974; Cobbold, 1976a and discussion above). A discussion of the various styles and significances of folds in anisotropic rocks is given by Price and Cosgrove (1990).

Bayly (1970, 1974) proposed methods for deriving information on viscosity contrast and anisotropy from the geometry of chevron folds in bilaminate materials, by considering relative hinge thickening and change in limb length (Bayly, 1970) and by estimates of the energy consumed in incremental shortening of chevron folds with distinct hinge regions and straight limb regions (Bayly, 1974). Many assumptions, including Newtonian viscosity, are involved in applying these methods and they have not been subsequently applied or tested in any significant way.

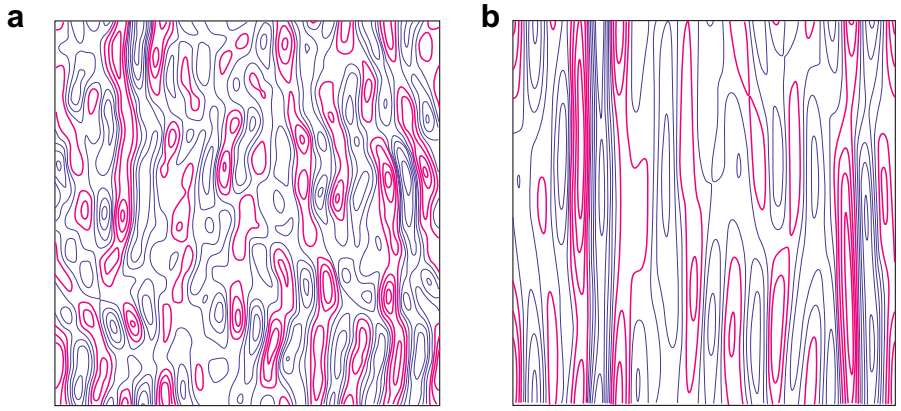

Fig. 23. Plan view in the plane of the layering showing the effects of selective amplification of initial, random perturbations in the folding of an isolated viscous layer ($n_L = 1.001$) in a viscous matrix with viscosity ratio, $\mu_L/\mu_M = 100$ after amplification of 100. Contours are normalized by the maximum height of the surface above its mid plane. The length of the side of the square region is 10 λ_d. (a) Newtonian layer, (b) power-law layer with $n_L = 10^4$ (Figs. 2D and 3D in Fletcher, 1995).

Chevron folds tend to develop in a multilayered sequence with stiff layers of similar thickness separated by thinner soft layers. Ramsay (1974) showed how characteristic modifications to the shape of the folds in the hinges, or accommodation structures, based on geometrical considerations and the assumption that the stiff layers tend to maintain constant length and thickness, were required if individual unusually thick layers are introduced. The typical accommodation structure is a keel-shaped or bulbous hinge zone (Ramsay, 1974, Fig. 8). This structure can also be produced when an unusual amount of slip is developed on the fold limbs in individual bedding planes (Price and Cosgrove, 1990, p. 319–321).

The large variation in shape of multilayer folds suggests that shape may potentially provide much more information on mechanical properties than has so far been achieved, but the fact that folds of a given shape can be arrived at by different processes and that layers of varying thickness and rheological properties may make up many multilayer fold packages makes realizing this difficult.

5. Strain measurement from folds

5.1. Elementary buckle shortening

For rock layers that have folded by buckling, the most elementary calculation of strain assumes that all the layer shortening is expressed in buckling. The bulk shortening stretch is the fold

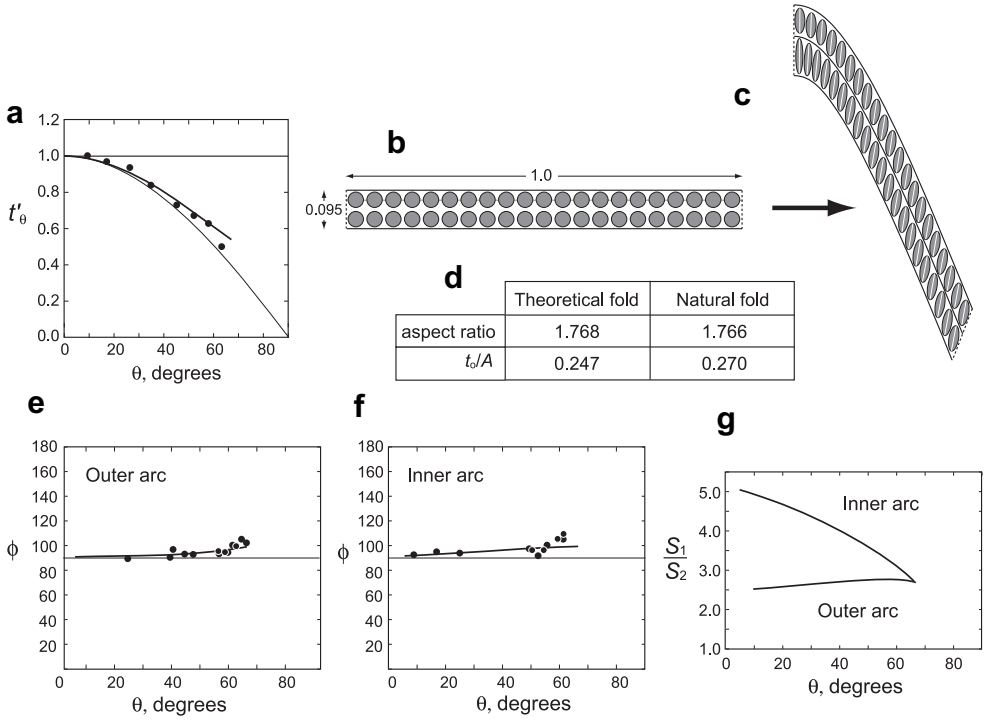

Fig. 24. Example of fit of a natural fold (not shown) by superposition of strain patterns applying the FoldModeler technique of Bobillo-Ares et al. (2004). (a) Ramsay's normalized thickness–dip (t'_θ *vs* θ) classification of theoretical folded layer (line) and natural fold (dots). (b) Initial configuration of theoretical layer. (c) Folded configuration of theoretical layer showing strain ellipses with long axis orientation, assumed to be parallel with cleavage. (d) Comparison of values of parameters of the modeled fold with corresponding values for the natural fold (aspect ratio is final amplitude/final width of the central (generating) fold surface; t_o is thickness at the hinge, A is the amplitude of the outer arc of the final fold. (e) and (f) Maximum stretch direction *vs* dip (φ–θ) diagrams for the outer and inner arcs respectively showing data obtained for the modeled folded layer (line) and natural fold (dots). (g) Strain ratio *vs* dip (S_1/S_2 *vs* θ) diagram for outer and inner arcs showing strain pattern predicted for theoretical fold (all data from Fig. 13, Bobillo-Ares et al., 2004).

'wavelength', or series of wavelengths (recognizing that quasi-periodic or non-periodic folds do not have wavelengths in the mathematical sense) (Fig. 4c or 17a) divided by the arclength, the same fold length measured around the folded layer. This method has been employed since some of the earliest studies of fold belts, including those of Claypole (1885), and Chamberlin (1910) in the Appalachians. The same principle is employed in line-length conservation in producing balanced and palinspastically restored cross sections in fold-and-thrust belts (Dahlstrom, 1969).

For one fold, with wavelength, λ, and the around-fold arclength, L, the shortening strain, e (-ve) and stretch, S (<1), are defined (Fig. 17):

$$S = (1 + e) = \lambda/L. \quad (16)$$

Measurements of λ and L must be made in a section perpendicular to the fold hinges, and the assumption is that there is no displacement gradient in the direction of the hinges.

5.2. Shortening according to fold shape

The method above assumes that all the layer shortening is expressed in buckling: i.e. there is no internal layer shortening preceding or accompanying folding. With this caveat, it is possible to determine the amount of shortening for folds of different shapes, such as sinusoids, circular arcs and types of angular folds (Currie et al., 1962, Fig. 7; Johnson, 1970, Fig. 4.3; Treagus, 1997, Fig. 19.2), as shown in Fig. 25. The relationships between stretch, S, and limb dip, α, are very simple and explicit for circular and chevron folds, but for a *sinusoid* of the form $y = m \sin x$, the stretch, S, cannot be expressed explicitly and involves an elliptic integral (Treagus, 1997).

These purely geometric approaches are useful in providing approximate or minimum bulk shortening for folds of a particular shape (Fig. 25). Pure buckling folds in single layers might be expected to follow the sinusoid curves more closely than the circular or chevron shapes (as demonstrated by Schmalholz and Podladchikov, 1999, for dips up to 50°) and these curves might be a good approximation for thin stiff layers with viscosity contrasts of $\geq$100.

5.3. Shortening in analog and numerical models

In an earlier review (Treagus, 1997), compilations of bulk model shortening versus fold limb dip in analog and numerical models (Fig. 26), sourced from a wide range of published fold studies, showed that there is commonly between ~5 and 20% bulk (layer-parallel) shortening before buckles start to amplify measurably (at around 10° limb dip), with the greater shortening for models with lower viscosity ratios. A comparison of Figs. 25 and 26a reveals that in the latter, the analog model with viscosity ratio = 100 (Hudleston, 1973a; Hudleston and Stephansson, 1973) is almost identical to curve S (sinusoid) in Fig. 25, if its origin is shifted to the 0.9 point (10% shortening). However, the numerical models in Fig. 26b show curves with a straighter trend at higher limb dip, as did several multilayer models not shown here.

5.4. Strain contour map of Schmalholz and Podladchikov

Schmalholz and Podladchikov (2001) provide a new method for estimating strain and viscosity contrast from fold shape, based on viscous and viscoelastic finite-amplitude fold modeling. The term, *fold shape*, does not here mean shape analysis as considered in section 4, nor the types of shape shown in Fig. 25. Instead, it concerns amplitude/wavelength (A/λ) and layer thickness/wavelength (h/λ) measurements plotted on a *strain contour map* (Schmalholz and Podladchikov, 2001, Fig. 6), as shown in Fig. 27. The theory and modeling behind this plot have been reviewed in section 2 above. For any natural or modeled fold where A/λ and h/λ can be measured, estimates of bulk strain (% shortening) and viscosity ratio (layer/matrix) can be read from the contour lines in Fig. 27. The strain is measured from the point at which the *nucleation amplitude* (see Section 2.2) is reached. It will be an underestimate if the initial amplitude is less than the nucleation amplitude and an overestimate if it is greater. In addition it is assumed that the fold initiated at the dominant wavelength. If it did not, the growth rate will be less than that assumed for the plot and thus the strain derived from it an underestimate. These underestimations or overestimations are likely to be small. Schmalholz and Podladchikov test their method against numerical and analog experiments in which the actual strain is known, and illustrate it with two examples of folded layers pictured in Ramsay and Huber (1987, Fig. 19.11) and Weiss (1972, plate 171). The A/λ and h/λ values for

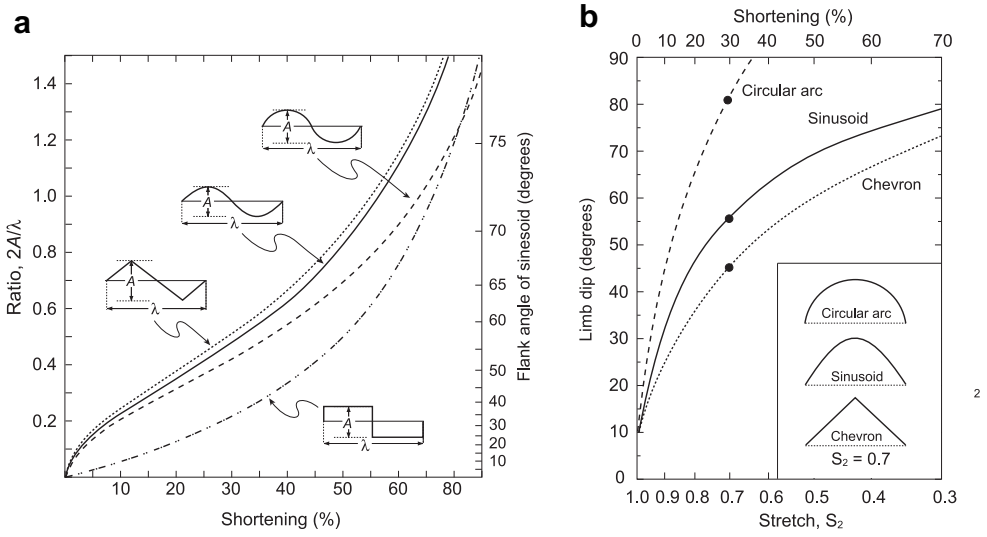

Fig. 25. (a) After Currie et al. (1962, Fig. 7). Amplitude/half-wavelength, $2A/\lambda$, and limb dip, θ, *vs* shortening for folds of different geometry - circular, sine, sawtooth and box. (b) Fig. 19.2 from Treagus (1997), of limb dip *vs* stretch for circular, sinusoidal and chevron folds.

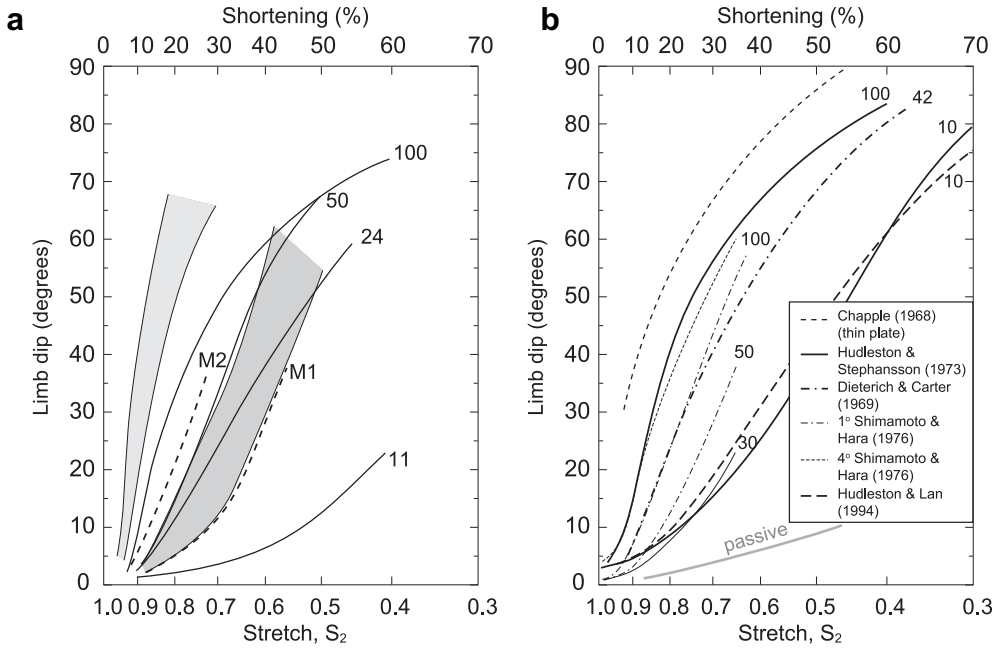

Fig. 26. (a) Compilation of data on changes of limb dip with shortening for analog models, from Treagus (1997, Fig. 19.4), with original data from Hudleston and Stephansson (1973) (solid lines – single-layer folds), Treagus (1972) (light shaded area – stiffer single layer folds with L/h of 11–15), (dark shaded area – softer single layer folds with L/h of 6–9). M1, M2 multilayers from Treagus (1972) (viscoplastic materials) and Johnson (1977) (elastic materials) respectively. (b) Compilation of data on limb dip *vs* shortening for single-layer folds developed in theoretical and numerical models by various authors, as indicated, from Treagus (1997, Fig. 19.5a). Numbers by each curve in (a) and (b) indicate viscosity ratio, μ_L/μ_M.

the former, given in Schmalholz and Podladchikov (2001, Table 2), lead to a strain determination of 70–72% shortening for this fold train; a significant shortening.

5.5. Scaled stretch and amplification, and stages of folding

Schmalholz (2006) provides another method of determining strain associated with stages of single layer folding, but does not measure the whole strain. This paper defines three stages of folding, termed *nucleation*, *amplification* and *kinematic growth*. Although reminiscent of Ghosh's *three stages of buckle folding* (Ghosh, 1993, p. 273) or three stages Treagus (1997) described as

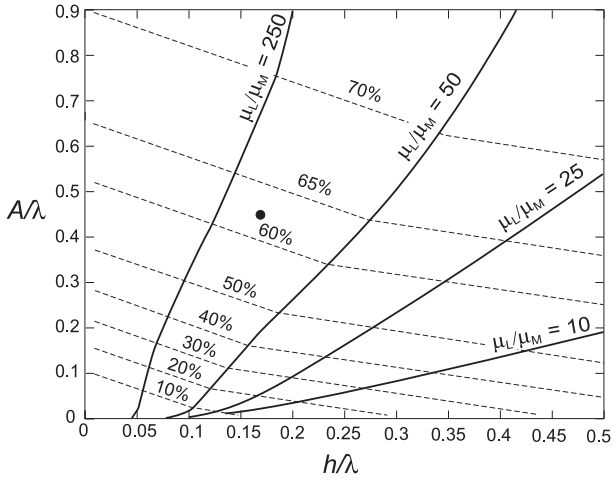

Fig. 27. The strain contour map – amplitude/wavelength (A/λ) plotted against thickness/wavelength (h/λ), from Schmalholz and Podladchikov (2001, Fig. 6), with contours showing bulk shortening and viscosity ratios. See Fig. 28 for an explanation of the black dot.

initial layer-parallel shortening, *active buckling*, and *late fold 'flattening'*, what distinguishes Schmalholz's (2006) approach is that the three stages are precisely defined (Fig. 16). Only the first stage has a variable degree of strain, which is related to the viscosity ratio and the initial amplitude. As reviewed earlier, Schmalholz presents a *scaled amplification equation*, which allows the *general amplification curve* to be drawn, as in Fig. 16. This approach derives from earlier papers (Schmalholz and Podladchikov, 2000, 2001) where the *crossover strain* and *crossover amplitude* were introduced that mark the change from the nucleation to amplification stage (see Sections 2.2, 3.1). Crossover strains may typically range from a few % (for large viscosity) to about 16% for the example in Fig. 16 (based on $\mu_L/\mu_M \approx 50$) and depend on the amplitude of the sinusoidal waveforms that make up the initial layer irregularities.

Schmalholz (2006) demonstrates that if the bulk shortening is normalized or "scaled" to the crossover strain, the 2nd and 3rd fold stages (amplification, and kinematic growth) have almost identical forms, for a range of viscosity ratios. However, the results appear to derive from initial growth rates (given by α_o in Schmalholz, 2006, Fig. 2, equal to q_o here) in the range of $q_o = 10$ to 26, that (according to Schmalholz and Podladchikov (2001), eq. (5), and taking $n_L = 1$) indicate viscosity ratios of 24–99. There must, therefore, be some caution in applying Fig. 16 to *all* single-layer folds, irrespective of other lines of evidence that might suggest viscosity ratios above or below this range.

Note that there are some inconsistencies in the definitions and notations in Schmalholz (2006, pp. 44–45). The *scaled stretch* (S_s in Fig. 16) needs to be clarified as the total stretch ($S > 1$) divided by the *crossover stretch* (not crossover strain), which would be better termed S_c (rather than e_C). It might be better to express the stretch values as <1, i.e. contractional, as these relate more obviously to % shortening strains associated with folding used by Schmalholz and Podladchikov (2001) and Schmalholz (2006). However, the $S > 1$ values have been retained in Fig. 16, to be faithful to these citations, and to follow the precedent set by Sherwin and Chapple (1968) and

Fletcher (1974), who expressed the strain associated with the initial layer-parallel shortening as $T = S_1/S_2, = 1/S_2^2$, in which S_2 is the stretch in Eq. (16). This convention is also used in Section 2.2.

The amplification stage of folding, defined by the amplitude/wavelength range of 0.05–0.15 (Fig. 16), is represented by a scaled stretch from 1 to 1.25, equivalent to 20% shortening for this stage. Beyond this, for limb dips of >45°, the fold continues to grow kinematically. This growth is not truly kinematic, since the analysis assumes that the arclength strains uniformly from inflexion to hinge, which will not be the case at high amplitudes, especially at low viscosity ratios.

We note that the amplification curve in Fig. 16 departs from the folding trends for $\mu_L/\mu_M = 50$ shown in Fig. 26, based on a range of earlier analog and theoretical viscous models. For folds with limb dips of 60° or 70°, Fig. 16 would lead to higher strain estimates than those given by the curve in Fig. 26. However, the significance of Schmalholz's new graph (Fig. 16) is that it defines the middle amplification stage of folding precisely, from scaled stretch of 1–1.25, regardless of viscosity ratio (within the limits stated above).

Schmalholz (2006) presents an example that combines this 'scaled stretch' method of strain estimation with the preceding Schmalholz and Podladchikov (2001) method, as shown in Fig. 28. The example is a folded quartz vein from Lisle (1995, p. 50). One fold has been selected and measured; its $A/\lambda = 0.45$ and $h/\lambda = 0.17$ values, plotted on the strain contour map (Fig. 27), determine the total shortening strain as 62%. These coordinates place the fold, spatially, between the $\mu_L/\mu_M = 50$ and 250 contours in Fig. 27, as indicated by the black dot on that figure. The A/λ value for this example is then used to plot this fold on the scaled stretch graph (Fig. 16). This indicates $S_s = 2.3$, equivalent to 57% shortening beyond the nucleation stage (from a scaled stretch value of 1.0 to one of 2.3). Hence, for this example (Fig. 28), the three fold stages emerge as: *nucleation*, 12% shortening (stretches 0.88 and 1.14) *amplification*, 20% further shortening (incremental stretches 0.8, 1.25) *kinematic growth*, 46% further shortening (incremental stretches 0.54, 1.85).

Multiplication of these three increments of stretch confirms the *total contractional stretch* of 0.38, i.e. 62% shortening, stated above.

6. Information on strain and deformation history from folded rocks

Theory and modeling have established that contraction of layered rocks will result in buckle folds. However, it does not follow that *all* folds in rocks are a result of simple shortening of layers, and isolated folds can arise through many mechanisms. Nevertheless, where a layer of rock is disposed in a train of folds of quite regular wavelength, such as discussed earlier, it is a reasonable assumption that the primary process is buckling in response to layer shortening. In section 5, we reviewed a number of methods of determining bulk shortening strain from natural buckle folds. In this section, we will consider what evidence folds might provide to indicate the deformation history for the folded layers, on a local or regional scale.

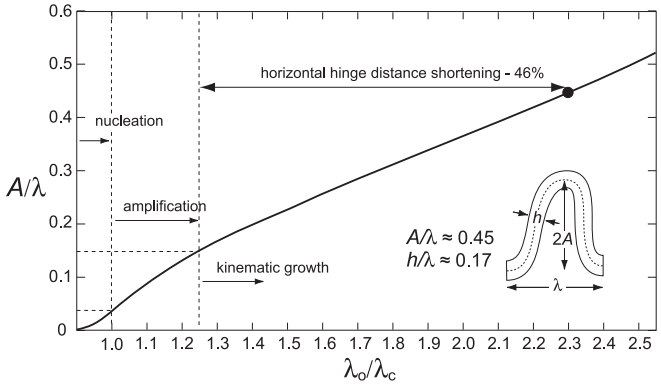

Fig. 28. Example of combining Figs. 16 and 27, after Schmalholz (2006, Fig. 8). The inset drawing and set of measurements are for a fold in a quartz vein taken from Lisle (1995). This fold is represented by an open circle on this plot and by a black dot on Fig. 27, where determination of the total strain is made. See text for stretch and strain values obtained for this fold.

6.1. Inferring fold mechanisms from strains and fabric (fanning and refraction of cleavage)

Two mechanisms for internal deformation associated with parallel folding have become classics in structural geology, used widely in text books and teaching: *flexural flow* and *tangential longitudinal strain* (Ramsay, 1967, pp. 391–398). These two mechanisms for accommodating strain in a layer without altering its thickness are shown in Fig. 29. *Flexural flow* (FF) has strain concentrated on limbs, and is analogous to bending a stack of paper (by sliding). *Tangential longitudinal strain* (TLS) has strain concentrated in the hinges, and is analogous to bending a continuous isotropic material such as rubber. Both fold mechanisms produce parallel folds (Class 1B, Ramsay, 1967, p. 366), with no change of orthogonal thickness (although there are intra-layer mutually compensating changes of thickening in the inner arc and thinning in the outer arc in the case of TLS), and have convergent dip isogons. However, the internal strain trajectories, and the cleavage traces – assuming cleavage is parallel to the *XY* plane of strain – are significantly different for FF and TLS fold mechanisms. One way of illustrating the difference is by making a combined isogon–strain classification of the folds (Treagus, 1982). Although this plot cannot represent the intensity of strain in folds, the orientations of strain trajectories or cleavage traces are sufficient to distinguish certain folding mechanism from others, such as FF from TLS. A variation of TLS is inner arc collapse, whereby there is no strain in the direction normal to layering, and all the folding is accommodated by layer-parallel shortening strain, associated with removal of material, most likely by pressure solution (Hudleston and Holst, 1984; Hudleston and Tabor, 1988). The principal strain orientations are the same as for TLS, but the neutral surface now lies at the outer arc of the fold.

Some of the earliest applications of *finite element* (FE) analysis in structural geology were used in the modeling of folds and revealed their deformation patterns. Dieterich (1969) and Dieterich and Carter (1969) first modeled the stress and strain patterns associated with folding of viscous single layers, and made comparisons with cleavage patterns in natural folds. Shimamoto and Hara (1976) used the FE method to examine the geometry and strain in single layer folds, and their results showed strain trajectories close to layer-orthogonal in the folded layer, indicating that tangential longitudinal strain is the dominant mechanism (see Fig. 29). There have been many subsequent FE studies of folding in single and multilayer folds (e.g. Lan and Hudleston, 1995b; Hudleston et al., 1996) that confirm the predominance of the TLS mechanism for viscous folding models. Hudleston and Holst (1984) analyzed strain in a folded limestone layer, and concluded that TLS was accompanied by some degree of inner-arc volume loss through pressure solution. Bobillo-Ares et al. (2000, 2006) considered compatibility issues associated with the TLS mechanism, and use kinematic and geometric modeling to examine the developments of strains, neutral surface and problems of area change. They conclude, illustrated by examples, that TLS folding in nature is not perfectly resolvable without the effects of area/volume changes and other geometrical effects in hinge regions, echoing some of the effects

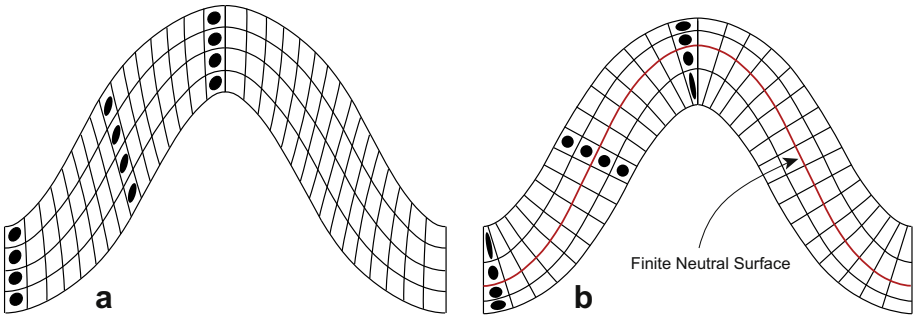

Fig. 29. Illustrations of flexural flow (a) and tangential longitudinal strain folds (b) showing strain ellipses (from Hudleston et al., 1996). The overall shape defined by the inner and outer arcs is identical in each case.

described for chevron folds (Ramsay, 1974; Bastida et al., 2007), considered below. According to Bobillo-Ares et al. (2006), the presence of radial wedged quartz veins in competent beds in fold outer arcs, and bulges or protuberances in inner arcs, are indicative of TLS processes in nature.

Returning to the alternative parallel folding mechanism, *flexural flow* (Fig. 29), we previously questioned FF as a valid mechanism for single layer folding (Hudleston et al., 1996), and concluded from FE models that such a layer would need to have a very high layer-parallel anisotropy ($\delta > 50$) to approach the FF mechanism. However, in a bilaminate multilayer that comprises alternating stiff and soft layers, if there are enough layers to represent the material as *statistically anisotropic*, the whole multilayer in bulk might be considered to have folded according to flexural flow. On a smaller scale, the alternating stiff and soft layers in the multilayer would fold by different mechanisms: the stiff layers approximately by TLS, as discussed above, with strain and fabrics concentrated in the hinge regions; the softer layers by a combination of flexural flow and strain accommodation; and the boundaries possibly by some degree of (flexural) slip. Fig. 30 shows typical patterns of alternating convergent and divergent cleavage fans, hinge fans and cleavage refraction that might be expected in folded multilayers of this kind, according to the strain patterns shown in FE models (Dieterich, 1969; Shimamoto and Hara, 1976), and models of strain fanning and refraction (Ramsay, 1967, p. 403; Roberts and Strömgård, 1972; Treagus, 1988, 1997). Such patterns (Fig. 30) are characteristically seen in interbedded sandstones/psammites and mudstones/pelites, in our experience (e.g. Fig. 31a,b).

The processes of folding in limestone/mudstone alternations, however, may be more complex than shown in Fig. 30. A study of three small folds by Ormand and Hudleston (2003) revealed

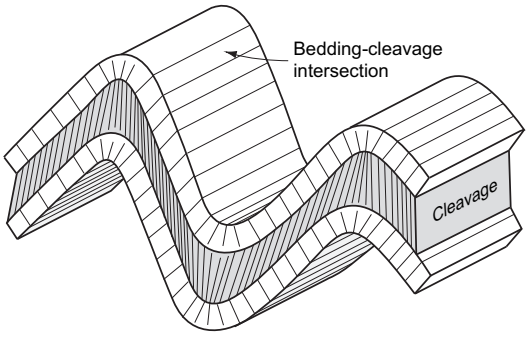

Fig. 30. Schematic typical cleavage fanning in fold hinges and refraction in limbs reflecting variations in strain developed in multilayers consisting of alternating stiff and soft members.

flexural flow as the predominant mechanism of single-layer folding, as well as variations according to scale. Considered together with the results of Hudleston and Holst (1984) discussed above, folded carbonate layers may exhibit a wide range of strain patterns and deformation mechanisms. Our earlier conclusion (Hudleston et al., 1996) that flexural flow is an unlikely mechanism for single-layer folding, except in highly anisotropic rocks, would appear to be contradicted in some instances in limestones.

The *flexural slip mechanism* (Tanner, 1989) is somewhat different from the mechanisms of folding discussed above. The essential characteristic is layer-parallel or bedding-plane slip, and flexural slip folding provides no additional definition of strain within the layers. Tanner's flexural slip folds are essentially *chevron folds*. They are defined mainly by slip between layers, indicated by geological features such as bedding-parallel veins, fractures and duplexes, plus slickenlines and slickenfibres that provide clear information on slip sense. In contrast, the Ramsay (1974) model for chevron folding has bonded layers, and deformation by variable amounts of flexural flow (FF) within the layers. Our own observations of chevron folds in alternating sedimentary sequences, especially the presence of convergent cleavage fans in hinge regions of competent beds and absence of strong strain fabrics on the limbs, not dissimilar from the patterns in Fig. 30, lead us to conclude that there is generally a significant component of tangential longitudinal strain in competent chevron fold hinge zones.

Bastida et al. (2007) provide kinematic models of chevron folds using a program, FoldModeler, to find the best combination of strain accommodation mechanisms in competent layers that can account for the observed strain and fabric patterns in natural chevron folds. They show that a sequence of different mechanisms is required for a good match, and that for angular folds with very strong curvature and narrow hinge zones, equiareal tangential longitudinal strain (ETLS) cannot be the exclusive mechanism in competent beds: other mechanisms and/or area change need to take place.

In the discussions above, we mainly use strain patterns and associated fabrics to infer the mechanisms of single or multilayer folding, but there are other geological structures and features that provide evidence for the deformation associated with folding. Veins, slickenlines and fibres and duplex fractures were referred to, above, in terms of evidence for bedding-plane slip and flexural slip (Tanner, 1989). Another important source of geological evidence is given by folding of layers that contain oblique markers or surfaces, such as folded cross-bedding or earlier fabrics (Williams, 1979; Aller et al., 2010; Bobillo-Ares et al., 2009). These last authors provide computer modeling of folding of two inclined surfaces by a range of mechanisms including FF and TLS plus 'flattening', to seek 'best fits' to natural examples. Their two examples of folded sandstone beds, one containing cross bedding, the other an earlier

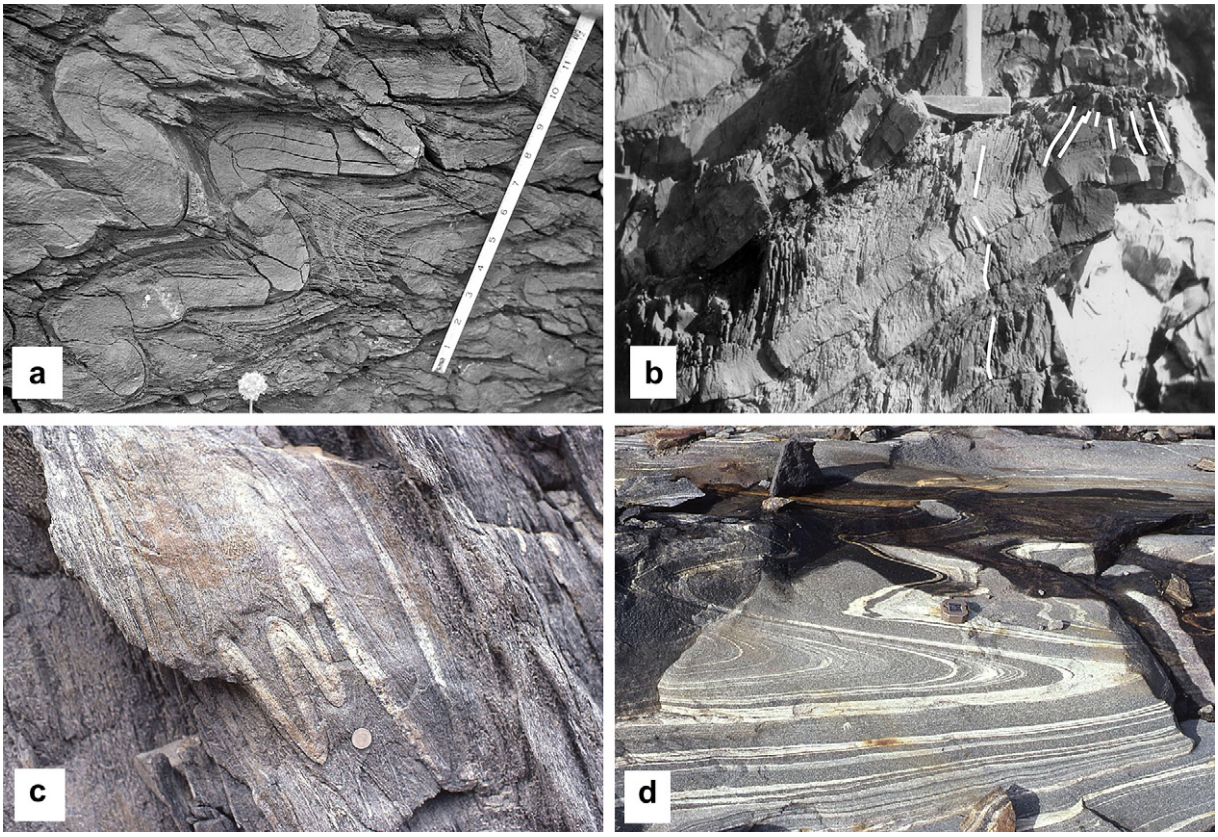

Fig. 31. (a) Buckle folds in siltstone layers in slates with cleavage that fans symmetrically about the fold axial surfaces, Boscastle, Cornwall, England; scale in inches. (b) Cleavage refraction through graded sandstone and mudstone beds on an anticlinal fold limb, Widemouth, Cornwall; hammer head 15 cm. The triangular cleavage fan at the hinge has been highlighted in white. (c) Flattened buckle folds in quartz-rich layer in schists, near Cap de Creus, Spain; coin 2.5 cm. (d) Largely passive similar folds in amphibolitic gneiss in highly sheared rocks at the base of a Caledonide basement thrust sheet, Swedish Lapland; compass 8 cm.

fabric, lead to the conclusion that folding was by a combination of mechanisms: flexural flow, tangential longitudinal strain and 'flattening'.

The concept of *fold flattening* and *flattened parallel folds* was introduced by Ramsay (1962a, 1967) to explain folds of class 1C geometry (e.g. Fig. 31c). Theoretical curves for different amounts of 'flattening' (homogeneous pure shear) of an initially parallel (1B) fold can be drawn within the 1C field of $t'-\alpha$ and *dip-isogon* fold classification graphs (Ramsay, 1967, Figs. 7–79; Hudleston, 1973c). Using examples of ptygmatic folded veins, Hudleston and Stephansson (1973, Fig. 9) revealed that the $t'-\alpha$ plots have close fits to flattening curves, but that the values of flattening deformation show quite a wide range, for different fold limbs in one fold train (strain ratios of 0.2–0.7), indicating inhomogeneous flattening on quite a small scale. In a similar way, Schmalholz and Podladchikov (2001), noted that not all folds in a layer grow to the nucleation amplitude simultaneously, depending on both initial amplitude and the initial wavelength. Thus folds in the same fold train can be at different points on the scaled amplification curve at the same time. In addition, for power-law materials the effective viscosity is a function of stress in the layer and this may vary if the folds grow asynchronously. Local development of serial folds may relieve stress in neighbouring sections and thus change the effective viscosity ratio (see Mancktelow, 1999). Folds at low viscosity contrasts may thus attain high amplitudes at different times and be subjected to different amounts of flattening at a late stage. Useful methods for estimating the flattening component of strain in initially parallel folds have been proposed by Srivastava and Shah (2006, 2008).

A large enough additional flattening or homogeneous pure shear imposed on a parallel (1B) fold would virtually transform it into a class 2, or similar fold (Fig. 31d). *Similar folds* (Ramsay, 1967, p. 421) are generally seen in ductile rocks where layering appears to have low viscosity contrasts, and deformation is great. They are also seen in salt and ice flows, where similar-style folds are shown by fine marker layers (Hudleston, 1976; Talbot, 1979; Talbot and Jackson, 1987). Whether such folds are the result of extreme flattening (homogeneous deformation) of weak buckling perturbations, or are a result of *differential simple shear* (Ramsay and Lisle, 2000, p. 825) may only be answered by examining their fabrics and strain patterns. A true axial-planar cleavage would suggest extreme flattening; divergent cleavages, in particular with asymmetrical development on either fold limb, suggest differential shear folding.

The *fanning and refraction of cleavage*, such as the patterns shown in Fig. 30 that can help to distinguish different mechanisms of folding, can be used in other ways. The sense of cleavage refraction across alternating competent and incompetent layers on folds limbs (e.g. Fig. 31a,b), can be used qualitatively to indicate relative increases and decreases of effective viscosity. To attempt to be quantitative, assumptions need to be made. For example, if it is assumed that cleavage approximately represents the principal *XY* plane of strain, for both competent and incompetent rocks, cleavage refraction can be taken as a direct indicator of strain refraction (Treagus, 1983, 1988). However, orientations of cleavage, alone, do not provide sufficient data to determine strain values, and thus are insufficient to determine effective viscosity ratios across boundaries. If, instead, it is assumed that cleavages initiated *before*

folding and are passively deformed bedding-orthogonal marker surfaces (Gray, 1981), the fans and refraction patterns could be used to determine the strain associated with folding. Treagus (1999) provided a possible compromise, and demonstrated that cleavage traces may be sufficiently close to deformed layer normals, under the conditions of folding and deformation, to provide a measure of shear strain across lithological boundaries, thus yielding information on effective viscosity ratios (which are the inverse of the shear-strain ratio). Examples are illustrated in Treagus (1999, Fig. 4) for using cleavage refraction on fold limbs (e.g. Fig. 31a,b) to estimate approximate viscosity ratios of greywacke/slate. A gradual change of cleavage orientation in a graded bed (e.g. Fig. 31b) can also indicate 'way up', a feature that can be useful in mapping of geological structures. In a related approach, Treagus et al. (2003) illustrated how the sense of cleavage refraction around a much-studied anticline in Britain helps to reveal its two-phase fold history and hinge migration.

6.2. Information from asymmetry of folds on different scales

Folds are seen on a variety of scales in orogenic belts, and a long-held method used by structural geologists in the field is to use the asymmetry and vergence of small-scale folds to indicate the geometry of larger-scale folds. In early to mid-20th Century structural geology texts, small-scale asymmetric folds were termed *drag folds* (e.g. Leith, 1923, p. 176; Billings, 1954, p. 78) and envisaged to be the result of shearing or flexural slip on larger-scale fold limbs, and were also termed *parasitic folds* (de Sitter, 1964, p. 279; Ramsay, 1967, p. 396). However, seminal papers by Ramberg (1963, 1964) established that asymmetric minor folds would have initiated as symmetrical fold waves, and become asymmetric by modification around larger-scale folds, by further shortening and layer-parallel shearing.

Treagus and Fletcher (2009) address the question of why small-scale folds initiate in multilayered rocks and are preserved in larger-scale folds in fold belts, when, as discussed in 2.4, theory and modeling have shown that multilayers comprising numerous layers will fold with a stronger amplification than a single or a few layers. This might suggest that large folds affecting numerous layers would fold more strongly than smaller folds affecting one or two layers, whereas field studies and minor-major fold relationships suggest the opposite. Treagus and Fletcher (2009) find that small folds in one layer are likely to outgrow larger multilayered folds, with the potential to become minor (parasitic) folds, if the thin layer is more competent than the rest, and/or if the multilayer is narrowly or stiffly confined. Fig. 15 illustrates the process, and the progressive change from initially symmetric to asymmetric minor (parasitic) folds around a major fold with progressive deformation, as classically proposed by Ramberg (1964). A natural example is shown in Fig. 32a, and strongly asymmetric folds that may lie on the flank of a larger fold in Fig. 32b. Other examples of folds on two or more different scales are shown in Figs. 1d and 2a.

Ghosh and Sengupta (2010) describe a somewhat different situation in which multilayer folds in mica schist sandwiched between more competent quartzite layers display the asymmetry of parasitic folds around the longer wavelength folds in the quartzite. It is the anisotropy of the mica schist in this case that results in internal folding (see Section 2.4), which has a greater buckling instability than the buckling of the quartzite layers in an anisotropic matrix.

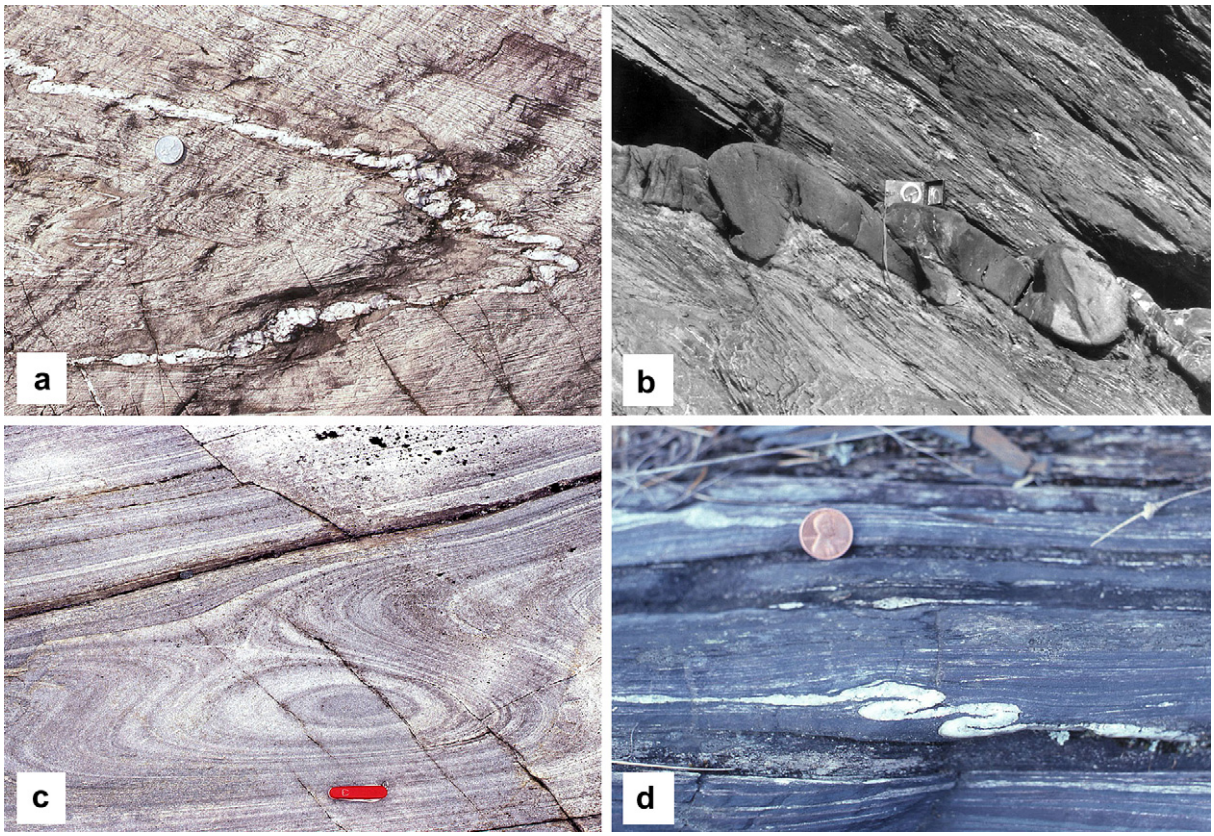

Fig. 32. (a) Parasitic folds in quartz vein in schist changing symmetry around a larger structure, Archean rocks near Geraldton, Ontario; coin 2.4 cm. (b) Strongly asymmetric buckle folds with thickened hinges and cleavage at a low angle to average bedding, in limestone layer in slates, Hele Bay, Devon, England; compass 15 cm. (c) Cross-section of sheath fold in quartzite in Caledonide cover nappes, Trollheimen, Norway; knife 9 cm. See Hansen (1971, Fig. 34) for a 3D representation of this fold pattern. (d) Asymmetric folds in quartz vein in iron-rich schist, reflecting the sense of displacement in a dextral shear zone, Archean rocks near Geraldton, Ontario; coin 1.9 cm.

Minor folds not only provide valuable information from their 'S' and 'Z' asymmetries (fold vergence; Bell, 1981) that reveal larger-scale and regional folds and aid geological mapping. Results in Treagus and Fletcher (2009) suggest that the relative scales of folding, and the presence of smaller with larger folds, can potentially provide information on the relationships of rheology and stratigraphy in multilayered rocks. This work ties together two classical studies and concepts: the *structural lithic units* of Currie et al. (1962); and *the orders of folding* of Ramberg (1964).

Most of this review has concentrated on the theory and modeling of buckle folds that develop in single or multiple layers that are parallel to the principal shortening deformation. The usual assumption is horizontal layering, horizontal shortening, and symmetric upright folds. However, folds in nature, even those that result from one phase of deformation, are rarely perfectly symmetrical. Large-scale fold asymmetry, and inclined fold axial planes, are common field observations and can have many explanations, some of which are suggested here. Local and variable asymmetry of buckle folds will be inherited from the initial perturbation spectrum, as seen in analog and numerical models (e.g. Figs. 10 and 14, Mancktelow, 2001). Perhaps the simplest reason for systematic fold asymmetry in the fold profile view, investigated by the second author many years ago (Beech, 1969; Treagus, 1972), is that the layers are oblique to the principal shortening, but parallel to the intermediate strain axis (*Y*). Layering is contracted but also undergoes rotation and shearing, progressively changing folds that initiate as symmetric waves (Treagus, 1973), into asymmetric folds (Anthony and Wickham, 1978). The fold axis would be expected to parallel *Y*, but the axial plane would initiate perpendicular to layering, and only approach the bulk *XY* plane when the folds are quite tight and asymmetric. Such a scenario might be initially dipping stratigraphy, such as on a continental shelf, undergoing subhorizontal crustal shortening. Buckle folds in a wedge-shaped fold-thrust belt would develop with a polarity and regional sense of overturning or vergence that reflects the asymmetry of and shear within the wedge (e.g. Rowan and Kligfield, 1992), and fault-related folds in fold-thrust belts are asymmetric reflecting the geometry and sequence of development of the thrusts with which they are associated. (e.g. Suppe, 1983, 1985)

Another major cause of fold asymmetry, which has important regional structural and tectonic implications, is folding associated with *shear zones*, discussed in the following section.

6.3. Folds in shear zones

Folds are commonly found in ductile shear zones, which are common in the mid to deep levels of the crust and in weak materials such as evaporites at higher levels. The strain gradients that define ductile shear zones may produce passive folds in layering that lacks significant rheological contrasts, and similar folds with axial surfaces sub-parallel to the shear zone boundaries reflect the combination of large shear strains with irregularities in the layering and low rheological contrasts (e.g. Fig. 31d, Hudleston, 1977; Carreras et al., 2005). Fold hinges typically form at a high angle to the shear direction, but with progressive strain, they tend to rotate towards parallelism with the shear direction (e.g. Escher and Watterson, 1974), in three dimensions forming sheath folds (e.g. Cobbold and Quinquis, 1980; Skjernaa, 1989; Fig. 32c), which are a key indicator of sense of shear in shear zones (e.g. Simpson, and Schmid, 1983; Hanmer and Passchier, 1991). Fold asymmetry is also used as a shear-sense indicator (e.g. Fig. 32d), but this must be applied with care, as reversals in apparent sense of shear can arise in a number of ways, as a result of large strains and 3D effects (Ramsay et al., 1983; Passchier and Williams, 1996; Alsop and Holdsworth, 2002). Carreras et al. (2005) provide a good review of the kinematics of folds of various types in shear zones.

Mechanical instabilities can lead to folding in layered or anisotropic rocks in shear zones. Buckling instabilities in single layers will exist if the layer is oblique to the shear zone boundary and there is a component of shortening parallel to the layer. Initially the folds produced are symmetric, and they become modestly asymmetric with increasing strain (Ghosh, 1966; Manz and Wickham, 1978). Asymmetry of cleavage refraction in the two limbs is more marked than the asymmetry of fold shape, with stronger refraction in the long limb than in the short limb (Viola and Mancktelow, 2005). In multilayered, effectively anisotropic media or homogeneous anisotropic media, folding instabilities exist, the effects of which depend on the orientation of the plane of anisotropy to the shear plane. The structures produced include kink bands, crenulations and shear bands. They have been studied experimentally (Ramberg and Johnson, 1976; Williams and Price, 1990; Mandal et al., 2004) and treated conceptually and analytically (Platt, 1983; Dennis and Secor, 1987; Fletcher, 2005). Fletcher (2005) showed that a weak instability existed even for the case of the plane of anisotropy parallel to the shear plane, although amplification is followed by deamplification as the structure rotates under the influence of the shear.

Flanking structures are isolated folds and shear bands associated with strain perturbation around veins, dikes or fractures in shear zones (Fig. 33a, Hudleston, 1989; Passchier, 2001; Grasemann and Stüwe, 2001). Since different mechanisms can produce these structures, care must be used when using them as sense of shear indicators (Passchier, 2001; Grasemann and Stüwe, 2001). Kocher and Mancktelow (2006) show that anisotropy significantly influences the development of flanking structures, which must be taken into account when considering these structures as shear sense indicators. They also suggest that the geometry of these structures may provide an estimate of the degree of anisotropy of rocks in shear zones.

6.4. Three-dimensional features of folds: localization, transected folds, and refolded folds

Until now, we have mainly concentrated on folds in single or multiple layers, in theory, models and naturally-deformed rocks, and with the assumption that the folds form by processes of buckling. The folds initiate as a series of sinusoidal-type waves that are explicable accordingly to buckling theory and modeling for the rheology concerned, as discussed in section 2. We would argue that this approach is valid for a wide range of geological settings for ductile rocks in orogenic belts. However, a geologist studying higher-level sedimentary rocks, upon discovering one or more folds, might come to a different conclusion. For him or her, the fold might be interpreted as an important localized structure, indicating faulting at depth or out of section. Buckling might not be regarded as the primary cause, unless a sequence of sinusoidal folds are seen. Folds that occur as localized features, whether they affect soft sediments (e.g. Woodcock, 1976), are forced or drape folds (e.g. Chester et al., 1988; Cook, 1988), or are variously fault-related (Suppe, 1983, 1985; McClay, 1992), provide important information about the conditions of the rock and the local deformation, but the varieties are too great to contain in this review. For *fault-related folds*, readers are referred to a Special Issue of this Journal (Wilkerson et al., 2002) for information and review.

Another example of localized folding would be the process of folding according to the thermal-mechanical feedback model of Hobbs et al. (2008), by which thermally induced weakening promotes buckling at low values of λ/h, with deformation concentrated in shear zones in the stiff layer connecting adjacent inner arc

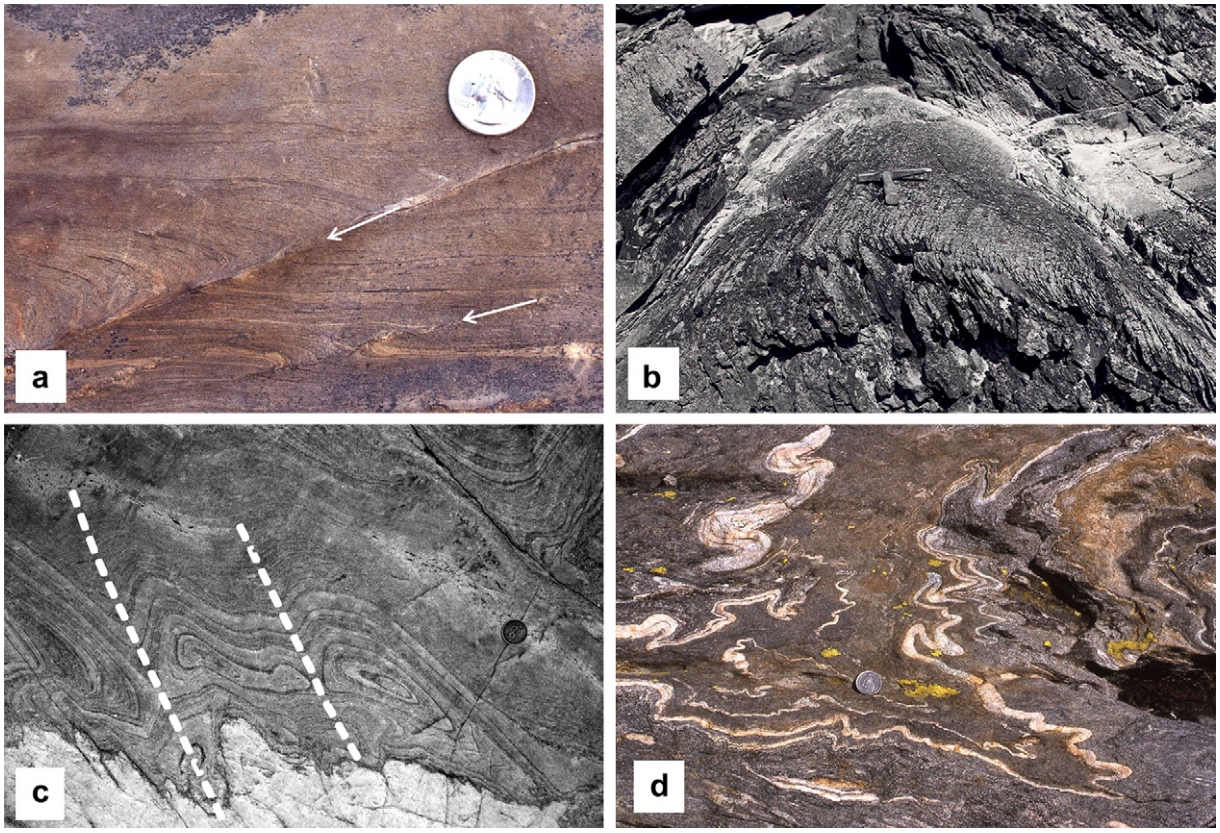

Fig. 33. (a) Flanking folds associated with rotated fractures/veins in a dextral shear zone in Archean biotite schist, Rainy Lake, Minnesota; coin 2.4 cm. White arrows indicate fractures about which flanking folds formed. (b) Cleavage-transected fold in sandstones and mudstones, Southern Uplands, Scotland (Stringer and Treagus, 1980, Fig. 5c); hammer head 18 cm. The hammer, parallel to the fold axis, is at a clear angle to the axial-planar cleavage. (c) F1/F2 fold interference marked by passive behavior of layers in Moine schists. Loch Monar, Scotland; coin 3 cm. Axial surface traces of 2 F2 folds marked by dashed lines. (d) F1/F2 fold interference complicated by buckling of white pegmatitic veins in both F1 and F2 deformations, Maggia nappe, Ticino, Switzerland; coin 2.3 cm.

fold hinges. We and others have recently discussed and questioned the validity of this model as a significant process of small-scale geological folding (Treagus and Hudleston, 2009; Hobbs et al., 2009, 2010; Schmid et al., 2010), and will not repeat the arguments here.

Folds in which the cleavage is observed to be oblique to the fold axis and axial plane, i.e. non-axial-planar, are termed *transected folds* (Borradaile, 1978; Stringer and Treagus, 1980). An example is shown in Fig. 33b. One explanation is buckle folding of layers that are oblique to all three principal directions of strain (Flinn, 1962; Treagus and Treagus, 1981): the fold axis for a 3D-oblique layer (parallel to the longer axis of the sectional ellipse) would not generally coincide with the intersection of the *XY* principal plane and the layer. For this type of oblique deformation, assuming cleavage forms parallel to the *XY* plane, the cleavage would be oblique to the axial plane. Treagus and Treagus (1981) investigated the structures that would be associated with folding of generally oblique layers in a triaxial strain ellipsoid, showing that transection angles (Borradaile, 1978) rarely exceed 10°, but increase from flattening to constrictional strain (i.e. with the strain ellipsoid shape factor; Flinn, 1965). As significant as the transection are the expected values for axial (hinge) migration, fold plunge variations, and the degree of cylindroidal or periclinal geometry, for layers folding in constrictional to flattening strain ellipsoids (Treagus and Treagus, 1981). Periclinal folding, strong plunge variations, and folding in two directions (cross folding) were suggested as indicators of folding in a constrictional deformation environment.

The occurrence of transected folds in the Caledonian-Appalachian orogenic belt (e.g. Fig. 33b), where the deformation is recognised to contain components of *transpression* (Harland, 1971; Sanderson and Marchini, 1984), has led to conclusions that clockwise-transected folds are direct evidence for sinistral transpressive deformation (Soper and Hutton, 1984; Soper et al., 1987; Woodcock et al., 1988), and vice versa. However, Treagus and Treagus (1992) questioned the theoretical basis for equating transected folds with transpression, and concluded that there is no obvious explanation for transected folds in horizontal layers in simple transpression (Harland, 1971; Sanderson and Marchini, 1984), unless cleavage does not does not track the finite *XY* plane of strain (see Soper, 1986). For the case where layers have different initial orientations (strikes and dips) with respect to a horizontal transpression, analogous to folding of oblique layers discussed above, transected folds would now be expected, but there is no simple relationship between, for example, clockwise transection and sinistral transpression: the relationships would vary according to the orientations of the folding layers (see Treagus and Treagus, 1992, for more examples and values).

We now turn to polyphase deformation, and the information that *polyphase and refolded folds* (e.g. Fig. 33c,d) can provide about the deformation of an area. The patterns of refolding and fold interference, classically described by O'Driscoll (1962a, 1962b) and Ramsay (1962b, 1967, chapter 10) and classified by Thiessen and Means (1980) and Grasemann et al. (2004), make up one of the modeling sessions in Ramsay and Lisle (2000, session 35). The two interfering fold phases are both modeled as sinusoidal fold-forming simple shear deformations (i.e. similar folds): the 'interference' map patterns are produced geometrically, without the involvement of mechanics of buckling. This is a useful way of determining the

characteristic geometry of fold interference (see Ramsay, 1967, Fig. 10–13) according to the relative orientations of the two fold phases: patterns such as egg-box, crescent, etc. However, it is known from analog experimental studies in systems with rheological contrasts (Ghosh and Ramberg, 1968; Watkinson, 1981; Odonne and Vialon, 1987; Ghosh et al., 1992, 1993, 1995; Grujic, 1993; Johns and Mosher, 1996; Sengupta et al., 2005), that the geometry of the 'first folds' will influence the 'second folds'. The studies by Ghosh and others reveal the 3D complexities that arise in interfering folds on different scales in materials with rheological contrasts. The folds shown in Fig. 33d involved buckling during two separate phases of deformation, this being mechanically easiest when, as here, folds of the two phases are coaxial.

Watkinson and Cobbold (1981) showed that earlier fold axes or lineations will act as a linear anisotropy, and may 'control' the orientation of later fold axes. Hence, it should not necessarily be assumed that the axis of later folding and small-scale fold hinges and crenulations, exactly reflect a position perpendicular to the maximum shortening direction for the later deformation. Nevertheless, and despite these reservations, the patterns of refolding, the presence of small-scale folds and crenulated fabrics, and the orientations of fold axes and fabrics of different generations provide a valuable resource for gaining information about regional deformations and tectonics, and have played a historically important part in documenting and unravelling the deformation of many parts of the Earth's crust (see Turner and Weiss, 1963 and Ramsay, 1967 for seminal examples of earlier work).

7. Future work

The mechanical processes that produce folds in rocks are now fairly well understood, based on a solid body of theoretical and modeling work, tied to a number of careful field studies. Questions remain, however. In the past dozen years or so, attention has been paid to possible elastic effects, in addition to the clear importance of viscous behavior, on fold development. If rocks behave in a viscoelastic manner (with Maxwell or more complex rheology) stress level or strain rate becomes important in determining how folds develop - if the strain rate or stress level is high enough - and nonlinear effects may become significant. It is not yet clear, however, if elastic properties are important in natural fold development, especially for the small-scale folds so common in most orogenic belts. It will be important to develop criteria that allow determination of whether or not elastic properties play a role in natural fold development. Some of the work reviewed here does suggest that such criteria may be developed. Other processes or phenomena that have been suggested as controlling fold development, including thermal-mechanical feedback, also need to be tested against well-constrained field examples.

The greatly increased power of modern computers allows increasingly realistic deformational scenarios to be modeled, and this offers the prospect that both forward and reverse modeling may be carried out in efforts to find the combination of rock properties and deformational conditions that best accounts for observed structures. With increasingly sophisticated tools to determine conditions of temperature, pressure and measurement of age, and thus strain rate, and increased ability to interpret microstructures in terms of rheological properties, strain rate and state of strain, the possibility exists of tightly constraining conditions of deformation and mechanical controls on natural folds.

Acknowledgments

We thank Cees Passchier for inviting us to contribute a review paper to mark JSG's 30th anniversary. It brought us together to write about one of our favorite topics, a happy reminder both of our research begun long ago at Imperial College, London, and of our shared time as former editors of JSG. We would like to thank John Ramsay for inspiring us to appreciate the beauty of folds, and Ray Fletcher for providing keen comments, interest and the sharing of ideas. PJH acknowledges earlier support from the National Science Foundation and support in various forms from the University of Minnesota. SHT acknowledges support for research from the NERC as a Senior Research Fellow and from the University of Manchester, and thanks Jack Treagus for his constant interest and encouragement over the years. Finally, we thank Neil Mancktelow and Sudipta Sengupta for their review comments that have been invaluable in helping us revise the paper.

Appendix. Symbols used

A	Amplitude
A_o	Initial amplitude
B	Constant in power law
$\dot{e}$	Strain rate
E_L/E_M	Elasticity (Young's modulus) ratio of layer to matrix
G	Elastic shear modulus
h	Thickness of individual layers
h_o	Initial thickness of individual layers
H	Thickness of multilayer package
k	Wave number, $k = 2\pi h/\lambda$
k_o	Initial wavenumber
Ki	Curvature index, defined in Fig. 18.
L	Arclength
L_o	Initial arclength
$\overline{L}/h$	Mean value of L/h for a fold population
n	Power law exponent
n^*	Effective power-law exponent in non-plane strain conditions
n_L, n_M	Power law exponents of layer and matrix
N	Number of stiff layers in a multilayer package, or total layers in a package
P	Layer-parallel compressive stress
$q(k)$	Growth factor
Q	Rheological parameter in Eq. (8), $Q = \sqrt{n_L}R''$
R	Ratio of viscous to elastic dominant wavelengths, $R = \lambda_{dv}/\lambda_{de}$
R'	Ratio of normal viscosities for anisotropic buckling, $R' = \mu_M'^n/\mu_L'^n$
R''	Effective viscosity ratio for anisotropic buckling, $R'' = \sqrt{\mu_M'^n \mu_M'^s}/\mu_L'^n$
s	Spacing of competent layers in a multilayer package
S	Stretch
S_1, S_2	Principal stretches in plane strain (the xz plane), with $S_1 \geq S_2$ and $S_1S_2 = 1$
Sc	Crossover stretch
Ss	Scaled stretch
t	Time
t'	Normalized thickness in Ramsay thickness-dip plot
T	Ratio of principal stretches, $T = S_1/S_2$
x,y,z	Coordinate system, with x parallel to the shortening direction in plane strain, z perpendicular to x in the plane of strain.
θ	Limb dip
α_1, α_2	Fractions of thicknesses of layers of viscosities μ_1 and μ_2 in multilayer package
α_L, β_L	Functions of n_L, defined in Eq. (9)
δ	Anisotropy factor, $\delta = \mu_n/\mu_s$
δ_L,δ_M	Anisotropy factors of layer and matrix

λ	Wavelength
λ_d	Dominant wavelength
λ_p	Preferred wavelength
λ_o	Initial wavelength
μ	Viscosity
μ_L,μ_M	Viscosities of layer and matrix
μ_n, μ_s	Normal and shear viscosities
μ_L^n,μ_L^s	Normal and shear viscosities of layer (and similar for matrix)
μ'_L and μ'_M	Viscosities under the base rate of flow
ν	Poisson's ratio
ξ	Ratio of strain rates in x and y directions, $\dot{e}_y/\dot{e}_x$, in buckling under non-plane strain
σ_x	Total normal stress in layer
$\overline{\sigma}_x$	Uniform normal stress in layer (membrane stress)
$\tilde{\sigma}_x$	Normal fiber stress in layer
τ	Dimensionless time, $\tau = -\dot{e}_x t$,
φ	Maximum stretch direction in fold profile

References

Abbassi, M.R., Mancktelow, N.S., 1990. The effect of initial perturbation shape and symmetry on fold development. Journal of Structural Geology 12, 273–282.

Aller, J., Bastida, F., Lisle, R.J., Ramsay, J.G., 2010. Photograph of the month: flexural slip folding of foresets in cross-bedded sandstones. Journal of Structural Geology, 725–726.

Alsop, G.I., Holdsworth, R.E., 2002. The geometry and kinematics of flow perturbation folds. Tectonophysics 350, 99–125.

Anthony, J.M., Wickham, J.S., 1978. Finite-element simulation of asymmetric folding. Tectonophysics 47, 1–14.

Bastida, F., Aller, J., Bobillo-Ares, N.C., 1999. Geometrical analysis of folded surfaces using simple functions. Journal of Structural Geology 21, 729–742.

Bastida, F., Aller, J., Bobillo-Ares, N.C., Toimil, N.C., 2005. Fold geometry; a basis for their kinematical analysis. Earth-Science Reviews 70, 129–164.

Bastida, F., Aller, J., Toimil, N.C., Lisle, R.J., Bobillo-Ares, N.C., 2007. Some considerations on the kinematics of chevron folds. Journal of Structural Geology 29, 1185–1200.

Bayly, M.B., 1970. Viscosity and anisotropy estimates from measurements on chevron folds. Tectonophysics 9, 459–474.

Bayly, M.B., 1974. An energy calculation concerning the roundness of folds. Tectonophysics 24, 291–316.

Beech, S.H., 1969. Buckling of single and multi-layers oblique to principal compressive stress, and its bearing on the problem of asymmetric fold formation. M.Sc. thesis (unpublished), Imperial College, University of London.

Bell, A.M., 1981. Vergence: an evaluation. Journal of Structural Geology 3, 197–202.

Billings, M.P., 1954. Structural Geology. Prentice-Hall Inc., New Jersey.

Biot, M.A., 1961. Theory of folding of stratified viscoelastic media and its implications in tectonics and orogenesis. Geological Society of America Bulletin 72, 1595–1620.

Biot, M.A., 1964. Theory of internal buckling of a confined multilayered structure. Geological Society of America Bulletin 75, 563–568.

Biot, M.A., 1965a. Mechanics of Incremental Deformations. John Wiley and Sons, New York.

Biot, M.A., 1965b. Theory of similar folding of the first and second kind. Geological Society of America Bulletin 76, 251–258.

Biot, M.A., 1965c. Further development in the theory of internal buckling of multilayers. Geological Society of America Bulletin 76, 833–840.

Biot, M.A., Ode, H., Roever, W.L., 1961. Experimental verification of the theory of folding of stratified viscoelastic media. Geological Society of America Bulletin 72, 1621–1632.

Bobillo-Ares, N.C., Bastida, F., Aller, J., 2000. On tangential longitudinal strain folding. Tectonophysics 319, 53–68.

Bobillo-Ares, N.C., Toimil, N.C., Aller, J., Bastida, F., 2004. FoldModeler; a tool for the geometrical and kinematical analysis of folds. Computers and Geosciences 30, 147–159.

Bobillo-Ares, N.C., Aller, J., Bastida, F., Lisle, R.J., Toimil, N.C., 2006. The problem of area change in tangential longitudinal strain folding. Journal of Structural Geology 28, 1835–1848.

Bobillo-Ares, N.C., Bastida, F., Aller, J., Lisle, R.J., 2009. An approach to folding kinematics from the analysis of folded oblique surfaces. Journal of Structural Geology 31, 841–852.

Borradaile, G.J., 1978. Transected folds: a study illustrated with examples from Canada and Scotland. Geological Society of America Bulletin 89, 481–493.

Burg, J.-P., Podladchikov, Y., 1999. Lithospheric scale folding: numerical modelling and application to the Himalayan syntaxes. International Journal of Earth Sciences 88, 190–200.

Carreras, J., Druguet, E., Griera, A., 2005. Shear zone-related folds. Journal of Structural Geology 27, 1229–1251.

Carter, N.L., Tsenn, M.C., 1987. Flow properties of continental lithosphere. Tectonophysics 136, 27–63.

Casey, M., Huggenberger, P., 1985. Numerical modelling of finite-amplitude similar folds developing under general deformation histories. Journal of Structural Geology 7, 103–114.

Chamberlin, R.T., 1910. The Appalachian folds of central Pennsylvania. Journal of Geology 18, 228–251.

Chapple, W.M., 1968. A mathematical theory of finite amplitude rock-folding. Geological Society of America Bulletin 79, 47–68.

Chester, J.C., Spang, J.H., Logan, J.M., 1988. Comparison of thrust fault rock models to basement-cored folds in the Rocky Mountain foreland. In: Schmidt, C.J., Perry Jr., W.J. (Eds.), Interactions of the Rocky Mountains Foreland and the Cordilleran Thrust Belt. Geological Society of America Memoir, vol. 171, pp. 65–74.

Claypole, E.W., 1885. Pennsylvania before and after the elevation of the Appalachian mountains, a study in dynamical geology. The American Naturalist 19, 257–268.

Cloetingh, S., Burov, E., Beekman, F., Andeweg, B., Andriessen, P.A.M., Garcia-Castellanos, D., de Vicente, G., Vegas, R., 2002. Lithospheric folding in Iberia. Tectonics 21 (5), 26.

Cobbold, P.R., 1975. Fold propagation in single embedded layers. Tectonophysics 27, 333–351.

Cobbold, P.R., 1976a. Mechanical effects of anisotropy during large finite deformation. Bulletin de la Société géologique de France 18, 1497–1510.

Cobbold, P.R., 1976b. Fold shapes as functions of progressive strain. Philosophical Transactions of the Royal Society A 283, 129–138.

Cobbold, P.R., 1977. The finite element analyses of fold propagation – problematic application. Tectonophysics 38, 339–353.

Cobbold, P.R., Quinquis, H., 1980. Development of sheath folds in shear regimes: Shear zones in rocks. Journal of Structural Geology 2, 119–126.

Cobbold, P.R., Cosgrove, J.W., Summers, J.M., 1971. Development of internal structures in deformed anisotropic rocks. Tectonophysics 12, 23–53.

Cook, D.G., 1988. Balancing basement-cored folds of the Rocky Mountains foreland. In: Schmidt, C.J., Perry Jr., W.J. (Eds.), Interactions of the Rocky Mountains Foreland and the Cordilleran Thrust Belt. Geological Society of America Memoir, vol. 171, pp. 53–64.

Cruikshank, K.M., Johnson, A.M., 1993. High amplitude folding of linear-viscous multilayers. Journal of Structural Geology 15, 79–94.

Currie, J.B., Patnode, H.W., Trump, R.P., 1962. Development of folds in sedimentary strata. Geological Society of America Bulletin 73, 655–674.

Czeck, D.M., Fissler, D.A., Horsman, E., Tikoff, B., 2009. Strain analysis and rheology contrasts in polymictic conglomerates: an example from the Seine meta-conglomerates, Superior Province, Canada. Journal of Structural Geology 31, 1365–1376.

Dahlstrom, C.D., 1969. Balanced cross sections. Canadian Journal of Earth Sciences 6, 743–757.

de Sitter, L.U., 1964. Structural Geology. McGraw Hill, New York.

Dennis, A.J., Secor, D.T., 1987. A model for the development of crenulations in shear zones with applications from the Southern Appalachian Piedmont. Journal of Structural Geology 9, 809–817.

Dieterich, J.H., 1969. Origin of cleavage in folded rocks. American Journal of Science 267, 155–165.

Dieterich, J.H., Carter, N.L., 1969. Stress history of folding. American Journal of Science 267, 129–154.

Escher, A., Watterson, J., 1974. Stretching fabrics, folds and crustal shortening. Tectonophysics 22, 223–231.

Fletcher, R.C., 1974. Wavelength selection in the folding of a single layer with power-law rheology. American Journal of Science 274, 1029–1043.

Fletcher, R.C., 1977. Folding of a single viscous layer: exact infinitesimal-amplitude solution. Tectonophysics 39, 593–606.

Fletcher, R.C., 1979. The shape of single-layer folds at small but finite amplitude. Tectonophysics 60, 77–87.

Fletcher, R.C., 1991. 3-dimensional folding of an embedded viscous layer in pure shear. Tectonophysics 13, 87–96.

Fletcher, R.C., 1995. 3-dimensional folding and necking of a power-law layer – are folds cylindrical, and if so, do we understand why? Tectonophysics 247, 65–83.

Fletcher, R.C., 2005. Instability of an anisotropic power-law fluid in a basic state of plane flow. Journal of Structural Geology 27, 1155–1167.

Fletcher, R.C., Sherwin, J., 1978. Arc lengths of single layer folds: a discussion of the comparison between theory and observation. American Journal of Science 278, 1085–1098.

Flinn, D., 1962. On folding during three-dimensional progressive deformation. Quarterly Journal Geological Society London 118, 385–433.

Flinn, D., 1965. Deformation in metamorphism. In: Pitcher, W.S., Flinn, G.W. (Eds.), Controls of Metamorphism. Geological Journal Special Issue No 1. Oliver and Boyd, Edinburgh and London, pp. 48–72.

Frehner, M., Schmalholz, S.M., 2006. Numerical simulations of parasitic folding in multilayers. Journal of Structural Geology 28, 1647–1657.

Gairola, V.K., Kern, H., 1984. Single-layer folding in marble and limestone: an experimental study. Tectonophysics 108, 155–172.

Ghosh, S.K., 1966. Experimental tests of buckling folds in relation to strain ellipsoid in simple shear deformations. Tectonophysics 3, 169–185.

Ghosh, S.K., 1968. Experiments on buckling of multilayers which permit interlayer gliding. Tectonophysics 6, 207–249.

Ghosh, S.K., 1993. Structural Geology: Fundamentals and Modern Developments. Pergamon, Oxford.

Ghosh, S.K., Ramberg, H., 1968. Buckling experiments on intersecting fold patterns. Tectonophysics 5, 89–105.

Ghosh, S.K., Sengupta, S., 2010. Paradoxical situation in determining relative competence from wavelength/arclength ratios within buckle folded multilayers. Journal of the Geological Society of India 75, 13–17.
Ghosh, S.K., Mandal, N., Khan, D., Deb, S.K., 1992. Modes of superposed buckling in single layers controlled by initial tightness of early folds. Journal of Structural Geology 14, 381–394.
Ghosh, S.K., Mandal, N., Sengupta, S., Deb, S.K., Khan, D., 1993. Superposed buckling in multilayers. Journal of Structural Geology 15, 95–111.
Ghosh, S.K., Khan, D., Sengupta, S., 1995. Interfering folds in constrictional deformation. Journal of Structural Geology 17, 1361–1373.
Grasemann, B., Stüwe, K., 2001. The development of flanking folds during simple shear and their use as kinematic indicators. Journal of Structural Geology 23, 715–724.
Grasemann, B., Wiesmayr, G., Dragantis, E., Fusseis, F., 2004. Classification of refold structures. Journal of Geology 112, 119–125.
Gray, D.R., 1981. Cleavage–fold relationships and their implications for transected folds: an example from southwest Virginia, U.S.A. Journal of Structural Geology 3, 265–277.
Grujic, D., 1993. The influence of initial fold geometry on Type 1 and Type 2 interference patterns: an experimental approach. Journal of Structural Geology 15, 293–307.
Grujic, D., Mancktelow, N.S., 1997. Folds with axes parallel to the extension direction; an experimental study. Journal of Structural Geology 17, 279–291.
Hall, J., 1815. On the vertical position and convolutions of certain strata and their relation with granite. Transactions Royal Society Edinburgh 7, 79–108.
Hanmer, S., Passchier, C., 1991. Shear-sense indicators; a review. Paper – Geological Survey of Canada 90-17, 72.
Hansen, E., 1971. Strain Facies. Springer-Verlag. New York.
Harland, W.B., 1971. Tectonic transpression in Caledonian Spitsbergen. Geological Magazine 108, 27–42.
Hills, E.S., 1963. Elements of Structural Geology. Methuen, London.
Hirth, G., Teyssier, C., Dunlap, W.J., 2001. An evaluation of quartzite flow laws based on comparisons between experimentally and naturally deformed rocks; Deformation mechanisms, rheology and microstructures. Geologische Rundschau – International Journal of Earth Sciences 90, 77–87.
Hobbs, B., Regenauer-Lieb, K., Ord, A., 2008. Folding with thermal-mechanical feedback. Journal of Structural Geology 30, 1572–1592.
Hobbs, B., Regenauer-Lieb, K., Ord, A., 2009. Folding with thermal-mechanical feedback: a reply. Journal of Structural Geology 31, 752–755.
Hobbs, B., Regenauer-Lieb, K., Ord, A., 2010. Folding with thermal-mechanical feedback: another reply. Journal of Structural Geology 32, 131–134.
Holst, T.B., 1987. Analysis of buckle folds from the early Proterozoic of Minnesota. American Journal of Science 287, 612–634.
Hudleston, P.J., 1973a. An analysis of "single layer" folds developed experimentally in viscous media. Tectonophysics 16, 189–214.
Hudleston, P.J., 1973b. An analysis and interpretation of minor folds in the Moine rocks of Monar, Scotland. Tectonophysics 16, 89–132.
Hudleston, P.J., 1973c. Fold morphology and some geometrical implications of theories of fold development. Tectonophysics 16, 1–46.
Hudleston, P.J., 1976. Recumbent folds in base of Barnes-Ice-Cap, Baffin Island, Northwest-Territories, Canada. Geological Society of America Bulletin 87, 1684–1692.
Hudleston, P.J., 1977. Similar folds, recumbent folds, and gravity tectonics in ice and rocks. Journal of Geology 85, 113–122.
Hudleston, P.J., 1986. Extracting information from folds in rocks. Journal of Geological Education 34, 237–245.
Hudleston, P.J., 1989. The association of folds and veins in shear zones. Journal of Structural Geology 11, 949–957.
Hudleston, P.J., Holst, T.B., 1984. Strain analysis and fold shape in a limestone layer and implications for layer rheology. Tectonophysics 106, 321–347.
Hudleston, P.J., Lan, L., 1993. Information from fold shapes. Journal of Structural Geology 15, 253–264.
Hudleston, P.J., Lan, L., 1994. Rheological controls on the shapes of single-layer folds. Journal of Structural Geology 16, 1007–1021.
Hudleston, P.J., Stephansson, O., 1973. Layer shortening and fold shape development in the buckling of single layers. Tectonophysics 17, 299–321.
Hudleston, P.J., Tabor, J.R., 1988. Strain and fabric development in a buckled calcite vein and rheological implications. Bulletin of the Geological Institutions of the University of Uppsala 14, 79–94.
Hudleston, P.J., Treagus, S.H., Lan, L., 1996. Flexural flow folding: does it occur in nature? Geology 24, 203–206.
Hunt, G.W., Mühlhaus, H.-B., Whiting, A.I.M., 1997. Folding processes and solitary waves in structural geology. Philosophical Transactions of the Royal Society London, A 355, 2197–2213.
Hunt, G., Mühlhaus, H., Hobbs, B., Ord, A., 1996. Localized folding of viscoelastic layers. Geologische Rundshau 85, 58–64.
Hunt, G.W., Edmunds, R., Budd, C.J., Cosgrove, J.W., 2006. Serial parallel folding with friction; a primitive model using cubic B-splines. Journal of Structural Geology 28, 444–455.
James, A.I., Watkinson, A.J., 1994. Initiation of folding and boudinage in wrench shear and transpression. Journal of Structural Geology 16, 883–893.
Jeng, F.S., Huang, K.P., 2008. Buckling folds of a single layer embedded in matrix – theoretical solutions and characteristics. Journal of Structural Geology 30, 633–648.
Jeng, F.S., Lai, Y.C., Teng, M.H., 2002. Influence of strain rate on buckle folding of an elasto-viscous single layer. Journal of Structural Geology 24, 501–516.
Johns, M.K., Mosher, S., 1996. Physical models of regional fold superposition: the role of competence contrast. Journal of Structural Geology 18, 475–492.
Johnson, A.M., 1970. Physical Processes in Geology. Freeman, Cooper and Company, San Francisco.
Johnson, A.M., 1977. Styles of Folding. Elsevier, New York.
Johnson, A.M., Fletcher, R.C., 1994. Folding of Viscous Layers. Columbia University Press, New York.
Johnson, A.M., Pfaff, V.J., 1989. Parallel, similar and constrained folds. Engineering Geology 27, 115–180.
Kaus, B.J.P., Schmalholz, S.M., 2006. 3D finite amplitude folding; implications for stress during crustal and lithospheric deformation. Geophysical Research Letters 33, L14309.
Kirby, S.H., Kronenberg, A.K., 1987. Rheology of the lithosphere; selected topics. Reviews of Geophysics 25, 1219–1244.
Kocher, T., Mancktelow, N.S., 2006. Flanking structure development in anisotropic viscous rock. Journal of Structural Geology 28, 1139–1145.
Kocher, T., Schmalholz, S.M., Mancktelow, N.S., 2006. Impact of mechanical anisotropy and power-law rheology on single layer folding. Tectonophysics 421, 71–87.
Kocher, T., Mancktelow, N.S., Schmalholz, S.M., 2008. Numerical modelling of the effect of matrix anisotropy orientation on single layer fold development. Journal of Structural Geology 30, 1013–1023.
Kohlstedt, D.L., Evans, B., Mackwell, S.J., 1995. Strength of the lithosphere; constraints imposed by laboratory experiments. Journal of Geophysical Research 100, 17,587–17,602.
Lan, L., Hudleston, P.J., 1991. Finite-element models of buckle folds in non-linear materials. Tectonophysics 199, 1–12.
Lan, L., Hudleston, P.J., 1995a. A method of estimating the stress exponent in the flow law for rocks using fold shape. Pure and Applied Geophysics 145, 621–635.
Lan, L., Hudleston, P.J., 1995b. The effects of rheology on the strain distribution in single layer buckle folds. Journal of Structural Geology 17, 727–738.
Lan, L., Hudleston, P., 1996. Rock rheology and sharpness of folds in single layers. Journal of Structural Geology 18, 925–931.
Latham, J.-P., 1979. Experimentally developed folds in a material with a planar mineral fabric. Tectonophysics 57, T1–T8.
Latham, J.-P., 1985a. The influence of nonlinear material properties and resistance to bending on the development of internal structures. Journal of Structural Geology 7, 225–236.
Latham, J.-P., 1985b. A numerical investigation and geological discussion of the relationship between folding, kinking and faulting. Journal of Structural Geology 7, 237–249.
Leith, C.K., 1923. Structural Geology. Henry Holt and Company, Inc., New York.
Lisle, R., 1995. Geological Structures and Maps: a Practical Guide. Butterworth-Heinemann, Oxford.
Lisle, R., 1997. A fold classification scheme based on a polar plot of inverse layer thickness. In: Sengupta, S. (Ed.), Evolution of Geological Structures in Micro to Macro-scales. Chapman & Hall, London, pp. 323–339.
Mancktelow, N.S., 1999. Finite-element modelling of single-layer folding in elasto-viscous materials; the effect of initial perturbation geometry. Journal of Structural Geology 21, 161–177.
Mancktelow, N.S., 2001. Single-layer folds developed from initial random perturbations; the effects of probability distribution, fractal dimension, phase, and amplitude. In: Koyi, H.A., Mancktelow, N.S. (Eds.), Tectonic Modeling: a Volume in Honor of Hans Ramberg. Geological Society of America Memoir, vol. 193, pp. 69–87.
Mancktelow, N.S., Abbassi, M.R., 1992. Single layer buckle folding in non-linear materials; II, Comparison between theory and experiment. Journal of Structural Geology 14, 105–120.
Mandal, N., Samanta, S.K., Chakraborty, C., 2004. Problem of folding in ductile shear zones; a theoretical and experimental investigation. Journal of Structural Geology 26, 475–489.
Manz, R.E., Wickham, J., 1978. Experimental analysis of folding in simple shear. Tectonophysics 44, 79–90.
McClay, K.R. (Ed.), 1992. Thrust Tectonics. Chapman Hall, London.
Mühlhaus, H.-B., Hobbs, B., Ord, A., 1994. The role of axial constraints on the evolution of folds in single layers. In: Siriwardane, Zaman (Ed.), Computer Methods and Advances in Geomechanics. Balkema, Rotterdam, pp. 223–231.
Mühlhaus, H.-B., Sakaguchi, H., Hobbs, B.E., 1998. Evolution of three-dimensional folds for a non-Newtonian plate in a viscous medium. Proceedings of the Royal Society London A 454, 3121–3143.
Mühlhaus, H.-B., Moresi, L., Hobbs, B., Dufour, F., 2002. Large amplitude folding in finely layered viscoelastic rock structures. Pure and Applied Geophysics 159, 2311–2333.
Neurath, C., Smith, R.B., 1982. The effect of material properties on growth rates of folding and boudinage: experiments with wax models. Journal of Structural Geology 4, 215–229.
Nevin, C.M., 1931. Principles of Structural Geology. Wiley, New York.
O'Driscoll, E.S., 1962a. Experimental patterns in superimposed similar folding. Journal of the Alberta Society of Petroleum Geologists 10, 145–167.
O'Driscoll, E.S., 1962b. Models for superposed laminar flow folding. Nature 196, 1146–1148.
Odonne, F., Vialon, P., 1987. Hinge migration as a mechanism of superimposed folding. Journal of Structural Geology 9, 835–844.
Ormand, C.J., Hudleston, P.J., 2003. Strain paths of three small folds from the Appalachian Valley and Ridge, Maryland. Journal of Structural Geology 25, 1841–1854.
Parrish, D.K., 1973. A nonlinear finite element fold model. American Journal of Science 273, 318–334.
Passchier, C.W., 2001. Flanking structures. Journal of Structural Geology 23, 951–962.

Passchier, C.W., Williams, P.R., 1996. Conflicting shear sense indicators in shear zones; the problem of non-ideal sections. Journal of Structural Geology 18, 1281–1284.
Paterson, M.S., Weiss, L.E., 1966. Experimental folding and deformation in phyllite. Geological Society of America Bulletin 77, 343–374.
Platt, J.P., 1983. Progressive refolding in ductile shear zones. Journal of Structural Geology 5, 619–622.
Price, N.J., Cosgrove, J.W., 1990. Analysis of Geological Structures. Cambridge University Press, Great Britain.
Ramberg, H., 1959. Evolution of ptygmatic folding. Norsk Geologisk Tiddskrift 39, 99–155.
Ramberg, H., 1960. Relationships between length of arc and thickness of ptygmatically folded veins. American Journal of Science 258, 36–46.
Ramberg, H., 1961. Contact strain and folding instability of a multilayered body under compression. Geologische Rundshau 51, 405–439.
Ramberg, H., 1963. Fluid dynamics of viscous buckling applicable to folding of layered rocks. Bulletin of the American Association of Petroleum Geologists 47, 484–505.
Ramberg, H., 1964. Selective buckling of composite layers with contrasted rheological properties, a theory for the simultaneous formation of several orders of folds. Tectonophysics 1, 307–341.
Ramberg, H., 1970. Folding of laterally compressed multilayers in the field of gravity, I. Physics of the Earth and Planetary Interior 2, 203–232.
Ramberg, H., 1981. Gravity, Deformation and the Earth's Crust, Second ed. Academic Press, London.
Ramberg, I.B., Johnson, A.M., 1976. A theory of concentric, kink and sinusoidal folding and of monoclinal flexuring of compressible, elastic multilayers; V, Asymmetric folding in interbedded chert and shale of the Franciscan Complex, San Francisco Bay area, California. Tectonophysics 32, 295–320.
Ramsay, J.G., 1962a. The geometry and mechanism of formation of "similar" type folds. Journal of Geology 70, 309–327.
Ramsay, J.G., 1962b. Interference patterns produced by the superposition of folds of similar type. Journal of Geology 70, 466–481.
Ramsay, J.G., 1967. Folding and Fracturing of Rocks. McGraw Hill, New York.
Ramsay, J.G., 1974. Development of chevron folds. Geological Society of America Bulletin 85, 1741–1754.
Ramsay, J.G., Huber, M.I., 1987. The Techniques of Modern Structural Geology. In: Folds and Fractures, vol. II. Academic Press, London.
Ramsay, J.G., Lisle, R.J., 2000. The Techniques of Modern Structural Geology. In: Applications of Continuum Mechanics in Structural Geology, vol. 3. Academic Press, London.
Ramsay, J.G., Casey, M., Kligfield, R., 1983. Role of shear in development of the Helvetic fold-thrust belt of Switzerland. Geology 11, 439–442.
Roberts, D., Strömgård, K.-E., 1972. A comparison of natural and experimental strain patterns around fold hinge zones. Tectonophysics 14, 105–120.
Rowan, M.G., Kligfield, R., 1992. Kinematics of large-scale asymmetric buckle folds in overthrust shear; an example from the Helvetic nappes. In: McClay, K.R. (Ed.), Thrust Tectonics. Chapman Hall, London, pp. 165–173.
Rutter, E.H., 1993. Experimental rock deformation; techniques, results and applications to tectonics. Geology Today 9, 61–65.
Sanderson, D.J., Marchini, W.R.D., 1984. Transpression. Journal of Structural Geology 6, 449–458.
Schmalholz, S.M., 2006. Scaled amplification equation: a key to the folding history of buckled viscous single-layers. Tectonophysics 419, 41–53.
Schmalholz, S.M., Mancktelow, N.S., 2008. Estimation of palaeo-rheology from buckle fold geometries. Bollettino Della Società Geologica Italiana 127, 227–230.
Schmalholz, S.M., Podladchikov, Y., 1999. Buckling versus folding: importance of viscoelasticity. Geophysical Research Letters 26, 2641–2644.
Schmalholz, S.M., Podladchikov, Y.Y., 2000. Finite amplitude folding: transition from exponential to layer length controlled growth. Earth and Planetary Science Letters 181, 619–633.
Schmalholz, S.M., Podladchikov, Y.Y., 2001. Strain and competence contrast estimation from fold shape. Tectonophysics 340, 195–213.
Schmalholz, S.M., Podladchikov, Y.Y., Schmid, D.D., 2001. A spectral/finite difference method for simulating large deformations of heterogeneous, viscoelastic materials. Geophysical Journal International 145, 199–208.
Schmid, D.W., Podladchikov, Y.Y., 2006. Fold amplification rates and dominant wavelength selection in multilayer stacks. Philosophical Magazine 86, 3409–3423.
Schmid, D.W., Dabrowski, M., Krotkiewski, M., 2008. Evolution of large amplitude 3D fold patterns; a FEM study; Recent advances in computational geodynamics; theory, numerics and applications. Physics of the Earth and Planetary Interiors 171, 400–408.
Schmid, D.W., Schmalholz, S.M., Mancktelow, N.S., Fletcher, R.C., 2010. Comment on 'Folding with thermal-mechanical feedback'. Journal of Structural Geology 32, 127–130.
Sengupta, S., Ghosh, S.K., Deb, S.K., Khan, D., 2005. Opening and closing of folds in superposed deformation. Journal of Structural Geology 27, 1282–1299.
Sherwin, J.-A., Chapple, W.M., 1968. Wavelengths of single layer folds: a comparison between theory and observation. American Journal of Science 266, 167–179.
Shimamoto, T., Hara, I., 1976. Geometry and strain distribution of single-layer folds. Tectonophysics 30, 1–34.
Simpson, C., Schmid, S.M., 1983. An evaluation of criteria to deduce the sense of movement in sheared rocks. Geological Society of America Bulletin 94, 1281–1288.
Skjernaa, L., 1989. Tubular folds and sheath folds; definitions and conceptual models for their development, with examples from the Grapesvare area, northern Sweden. Journal of Structural Geology 11, 689–703.
Smith, R.B., 1975. Unified theory of the onset of folding, boudinage, and mullion structure. Geological Society of America Bulletin 86, 1601–1609.
Smith, R.B., 1977. Formation of folds, boudinage, and mullions in non-Newtonian materials. Geological Society of America Bulletin 88, 312–320.
Smith, R.B., 1979. The folding of a strongly non-Newtonian layer. American Journal of Science 279, 272–287.
Soper, N.J., 1986. Geometry of anastomosing solution cleavage in transpression zones. Journal of Structural Geology 8, 937–940.
Soper, N.J., Hutton, D.H.W., 1984. Late Caledonian sinistral displacements in Britain: implications for a three-plate collision model. Tectonics 3, 781–794.
Soper, N.J., Webb, B.C., Woodcock, N.H., 1987. Late Caledonian (Acadian) transpression in north-west England: timing, geometry, and geotectonic significance. Proceedings of the Yorkshire Geological Society 46, 175–192.
Srivastava, D.C., Lisle, R.J., 2004. Rapid analysis of fold shape using Bezier curves. Journal of Structural Geology 26, 1553–1559.
Srivastava, D.C., Shah, J., 2006. A rapid method for strain estimation from flattened parallel folds. Journal of Structural Geology 28, 1–8.
Srivastava, D.C., Shah, J., 2008. The `isogon rosette` method for rapid estimation of strain in flattened folds. Journal of Structural Geology 30, 444–450.
Stabler, C.L., 1968. Simplified Fourier analysis of fold shapes. Tectonophysics 6, 343–350.
Stringer, P., Treagus, J.E., 1980. Non-axial planar S_1 cleavage in the Hawick rocks of the Galloway area, southern Uplands, Scotland. Journal of Structural Geology 2, 317–331.
Suppe, J., 1983. Geometry and kinematics of fault-bend folding. American Journal of Science 283, 684–721.
Suppe, J., 1985. Principles of Structural Geology. Prentice Hall, New Jersey.
Talbot, C.J., 1979. Fold trains in a glacier of salt in southern Iran. Journal of Structural Geology 1, 5–18.
Talbot, C.J., Jackson, M.P.A., 1987. Internal kinematics of salt diapirs. Bulletin of the American Association of Petroleum Geologists 71, 1068–1093.
Tanner, P.W.G., 1989. The flexural-slip mechanism. Journal of Structural Geology 11, 635–655.
Tentler, T., 2001. Experimental study of single layer folding in nonlinear materials. In: Koyi, H.A., Mancktelow, N.S. (Eds.), Tectonic Modeling: a Volume in Honor of Hans Ramberg. Geological Society of America Memoir, vol. 193, pp. 89–99.
Thiessen, R.L., Means, W.D., 1980. Classification of fold interference patterns: a reexamination. Journal of Structural Geology 2, 311–316.
Treagus, S.H., 1972. Processes in Fold Development. Ph.D. thesis, University of Manchester, Unpublished.
Treagus, S.H., 1973. Buckling stability of a viscous single-layer system oblique to the principal compression. Tectonophysics 19, 271–289.
Treagus, S.H., 1982. A new isogon – cleavage classification and its application to natural and model fold studies. Geological Journal 17, 49–64.
Treagus, S.H., 1983. A new theory of finite strain variation through contrasting layers, and its bearing on cleavage refraction. Journal of Structural Geology 5, 351–358.
Treagus, S.H., 1988. Strain refraction in layered systems. Journal of Structural Geology 10, 517–527.
Treagus, S.H., 1993. Flow variations in power-law multilayers: implications for competence contrasts in rocks. Journal of Structural Geology 15, 423–434.
Treagus, S.H., 1997. Modelling deformation partitioning in folds. In: Sengupta, S. (Ed.), Evolution of Geological Structures in Micro to Macro-scales. Chapman & Hall, London, pp. 341–372.
Treagus, S.H., 1999. Are viscosity ratios of rocks measurable from cleavage refraction? Journal of Structural Geology 20, 895–901.
Treagus, S.H., Fletcher, R.C., 2009. Controls of folding on different scales in multilayered rocks. Journal of Structural Geology 31, 1340–1349.
Treagus, S.H., Hudleston, P.J., 2009. Folding with thermal-mechanical feedback: discussion. Journal of Structural Geology 31, 749–751.
Treagus, J.E., Treagus, S.H., 1981. Folds and the strain ellipsoid; a general model. Journal of Structural Geology 3, 1–17.
Treagus, S.H., Treagus, J.E., 1992. Transected folds and transpression: how are they associated? Journal of Structural Geology 14, 361–367.
Treagus, S.H., Treagus, J.E., 2002. Studies of strain and rheology of conglomerates. Journal of Structural Geology 24, 1541–1567.
Treagus, S.H., Treagus, J.E., Droop, G.T.R., 2003. Superimposed deformations and their hybrid effects: the Rhoscolyn Anticline unravelled. Journal of the Geological Society 160, 117–136.
Turcotte, D.L., Schubert, G., 1982. Geodynamics. John Wiley & Sons Inc, New York.
Turner, F.J., Weiss, L.E., 1963. Structural Analysis of Metamorphic Tectonites. McGraw-Hill, New York.
Twiss, R.J., 1988. Description and classification of folds in single surfaces. Journal of Structural Geology 10, 607–623.
Van Hise, C.R., 1894. Principles of North American Pre-Cambrian geology. United States Geological Survey 16th Annual Report, 581–843.
Viola, G., Mancktelow, N.S., 2005. From XY tracking to buckling; axial plane cleavage fanning and folding during progressive deformation. Journal of Structural Geology 27, 409–417.
Watkinson, A.J., 1975. Multilayer folds initiated in bulk plane strain, with the axis of no change perpendicular to the layering. Tectonophysics 28, T7–T11.
Watkinson, A.J., 1981. Patterns of fold interference: influence of early fold shapes. Journal of Structural Geology 3, 19–23.

Watkinson, A.J., Cobbold, P.R., 1981. Axial directions of folds in rocks with linear/planar fabrics. Journal of Structural Geology 3, 211–217.
Weiss, L.E., 1972. The Minor Structures of Deformed Rocks. Springer, New York.
Wilkerson, M.S., Fischer, M.P., Apotria, T., 2002. Fault-related folds: the transition from 2-D to 3-D. Special issue. Journal of Structural Geology 24 (4).
Williams, P.F., 1979. The development of folds in a cross-laminated siltstone. Journal of Structural Geology 1, 19–30.
Williams, P.F., Price, G.P., 1990. Origin of kinkbands and shear-band cleavage in shear zones; an experimental study. Journal of Structural Geology 12, 145–164.
Willis, B., 1891. Mechanics of the Appalachian structure. United States Geological Survey 13th Annual Report, 212–281.
Woodcock, N.H., 1976. Structural style in slump sheets; Ludlow series, Powys, Wales. Journal of the Geological Society of London 132, 399–415.
Woodcock, N.H., Awan, M.A., Johnson, T.E., Mackie, A.H., Smith, R.D., 1988. Acadian tectonics in Wales during Avalonia/Laurentia convergence. Tectonics 7, 483–495.
Zhang, Y., Hobbs, B.E., Ord, A.M., Mühlhaus, H.B., 1996. Computer simulation of single layer buckling. Journal of Structural Geology 18, 643–655.
Zhang, Y., Mancktelow, N.S., Hobbs, B.E., Ord, A.M., Mühlhaus, H.B., 2000. Numerical modelling of single-layer folding: clarification of an issue regarding the possible effect of computer codes and the influence of initial irregularities. Journal of Structural Geology 22, 1511–1522.